HYDROTHERMAL SYNTHESIS AND CHARACTERIZATION OF VANADIUM AND TUNGSTEN OXIDE CONTAINING ORGANIC-INORGANIC HYBRID MATERIAL

A Thesis Submitted to
the Graduate School of Engineering and Sciences of
İzmir Institute of Technology
in Partial Fulfillment of the Requirements for the Degree of

MASTER OF SCIENCE

in Chemistry

by
Banu ÖNEN

July 2011
İZMİR

We approve the thesis of **Banu ÖNEN**

_____

Assoc. Prof. Dr. Mehtap EANES
Supervisor

_____

Assoc. Prof. Dr. Funda DEMİRHAN
Committee Member

_____

Assist. Prof. Dr. Şebnem E. SÖZERLİ
Committee Member

4 July 2011

_____

Prof. Dr. Serdar ÖZÇELİK
Head of the Department of Chemistry

_____

Prof. Dr. Durmuş Ali DEMİR
Dean of the Graduate School of
Engineering and Sciences

ACKNOWLEDGEMENTS

I would like to thank my supervisor Assoc. Prof. Dr. Mehtap EMİRDAĞ EANES for her support, encouragement and kindness during my master program.

I would also thank to TÜBİTAK 109T903 Project for financial support throughout this thesis.

I am thankful to İYTE-MAM researchers Duygu OĞUZ KILIÇ, Gökhan ERDOĞAN, Evrim YAKUT and Mine BAHÇECİ for their great help in my SEM, XRD and TGA analyses. I also thank Dr. Hüseyin ÖZGENER for providing help on FT-IR analyses.

My special thanks belong to my roommates, especially Leyla ERAL DOĞAN and Nesrin HORZUM POLAT for their support, help and friendship. I would also thank all my friends in İYTE, particularly Merve DEMİRKURT, Esen DÖNERTAŞ, Doğan TAÇ and Taylan MEŞİN for their understanding, friendship and help.

Finally, I am really grateful to my family; my mother Nazmiye ÖNEN, my father Teoman ÖNEN and my brother Berkay ÖNEN for their endless support, patience and love.

I would like to dedicate this thesis to my family and my grandfather Halil YETİM.

ABSTRACT

HYDROTHERMAL SYNTHESIS AND CHARACTERIZATION OF VANADIUM AND TUNGSTEN OXIDE CONTAINING ORGANIC-INORGANIC HYBRID MATERIAL

Hydrothermal synthesis of transition metal oxide containing organic-inorganic hybrid materials has attracted great attention recently.

Two novel organic-inorganic hybrid materials (4,4'-bipy)$_3$[$HPW_{12}O_{39}$] and [Cu(4,4'-bipy)$_4$][$HPW_{12}O_{40}$] were hydrothermally synthesized as green and purple crystals respectively, from the reaction of $Na_6[H_2W_{12}O_{40}]$, $CuCl_2.2H_2O$, 4,4'- bipyridine and H_3PO_4 in a 23 ml autoclave at 170°C for 72 hours. The compound (4,4'-bipy)$_3$[$HPW_{12}O_{39}$] crystallizes in the space group $P2_1/n$ of the monoclinic system with four formula units in a cell with dimensions a = 13.503(3) Å, b = 26.726(5) Å, c = 15.169(3) Å and V = 5397.3(19) Å^3. [Cu(4,4'-bipy)$_4$][$HPW_{12}O_{40}$] crystallizes in the space group P*bcn* of the tetragonal system with eight formula units in a cell of dimensions a = 20.236(4) Å, b = 25.635(5) Å, c = 20.236(4) Å; V = 10497(4) Å^3 . Both of the compounds are Keggin polyoxometalate structures. (4,4'-bipy)$_3$[$HPW_{12}O_{39}$] contains free 4,4'-bipy groups among the clusters while in [Cu(4,4'-bipy)$_4$][$HPW_{12}O_{40}$] 4,4'-bipy ligands are coordinated to Cu^{2+} ions.

A novel compound $(H_2NC_4H_8NH_2)[(VO)_2(PO_4)_2]$ was synthesized hydrothermally from the reaction of $NaVO_3$**,** V_2O_5, ethylenediamine and H_3PO_4 at 170°C for 72 hours. The compound crystallizes in the space group P-1 of the trigonal system with five formula units in a cell of dimensions a= 6.3345(13) Å, b= 6.3353(13) Å, c= 15.940(3) Å, V=639.6(2) Å^3. $(H_2NC_4H_8NH_2)[(VO)_2(PO_4)_2]$ displays a layered structure with protonated piperazine groups between layers.

In addition to the novel compounds, several known compounds were synthesized as well. Blue crystals of $(VO)(H_2PO_4)_2$ were obtained hydrothermally from the reaction of $NaVO_3$, ethylenediamine and H_3PO_4 at 170°C for 72 hours.

$(C_5NH_6)_{4.5}(H_3O)_{1.5}[P_2W_{18}O_{62}]$, a known compound also, was synthesized from the reaction of $Na_2WO_4.2H_2O$, $CuCl_2.2H_2O$, pyridine and H_3PO_4 at 170°C for 72 hours.

ÖZET

VANADYUM VE TUNGSTEN OKSİT İÇEREN ORGANİK-İNORGANİK MELEZ MALZEMELERİN HİDROTERMAL SENTEZİ VE KARAKTERİZASYONU

Geçiş metal oksitleri içeren organik-inorganik melez malzemelerin hidrotermal yöntemle sentezi son zamanlarda büyük ölçüde ilgi çekmektedir.

Yeni birer organik-inorganik melez malzeme olan yeşil renkli (4,4'-bipy)$_3$[$HPW_{12}O_{39}$] ve mor renkli [Cu(4,4'-bipy)$_4$][$HPW_{12}O_{40}$] tek kristalleri, 23 ml'lik otoklavlarda 170°C sıcaklıkta, 72 saatte, $Na_6[H_2W_{12}O_{40}]$, $CuCl_2.2H_2O$, 4,4'- bipiridin ve H_3PO_4 reaktantlarının hidrotermal koşullarda reaksiyona girmesi sonucu elde edilmişlerdir. (4,4'-bipy)$_3$[$HPW_{12}O_{39}$] kristali, monoklinik kristal sisteminin $P2_1/n$ uzay grubunda olup, dört formül birimi içeren ve boyutları a = 13.503(3) Å, b = 26.726(5) Å, c = 15.169(3) Å ve hacmi(V) 5397.3(19) Å^3 olan birim hücrede kristallenmiştir. [Cu(4,4'-bipy)$_4$][$HPW_{12}O_{40}$] ise, tetragonal sistemin P*bcn* uzay grubunda, sekiz formül birimine sahip, boyutları a = 20.236(4) Å, b = 25.635(5) Å, c = 20.236(4) Å; V = 10497(4) Å^3 olan birim hücreye sahiptir. Her iki malzeme de Keggin polioksometal yapısındadır. (4,4'-bipy)$_3$[$HPW_{12}O_{39}$] yapısında bulunan bipiridinler serbest haldeyken, [Cu(4,4'-bipy)$_4$][$HPW_{12}O_{40}$] malzemesinde, Cu^{2+} iyonlarıyla compleks yapmıştır.

Yeni bir organik-inorganik melez madde olan $(H_2NC_4H_8NH_2)[(VO)_2(PO_4)_2]$, $NaVO_3$, V_2O_5, etilendiamin ve H_3PO_4 maddelerinin 170°C sıcaklıkta, 72 saatte hidrotermal reaksiyonundan elde edilmiştir. Madde, triklinik kristal sisteminin P-*1* uzay grubunda beş formül birimine sahip ve boyutları a = 6.3345(13) Å, b = 6.3353(13) Å, c = 15.940(3) Å; V = 639.6(2) Å^3 olan birim hücrede kristallenmiştir. $(H_2NC_4H_8NH_2)[(VO)_2(PO_4)_2]$, katmanlı bir yapıya sahiptir ve bu katmanlar arasına protanlanmış piperazin grupları yerleşmiştir.

Yapılan çalışma sırasında, yeni malzemelerin yanı sıra bilinen malzemeler de sentezlenmiştir. Mavi çubuklar şeklinde elde edilen $(VO)(H_2PO_4)_2$; $NaVO_3$, etilendiamin ve H_3PO_4'in 170°C sıcaklıkta ve 72 saatte hidrotermal koşullar altında reaksiyona girmesi sonucunda sentezlenmiştir.

$(C_5NH_6)_{4.5}(H_3O)_{1.5}[P_2W_{18}O_{62}]$ organik-inorganik melez malzemesi de, $Na_2WO_4.2H_2O$, $CuCl_2.2H_2O$, piridin ve H_3PO_4'in 170°C sıcaklıkta, 72 saatte hidrotermal koşullarda reaksiyonu sonucunda elde edilmiştir.

TABLE OF CONTENTS

LIST OF FIGURES

Figure **Page**

LIST OF TABLES

CHAPTER 1

INTRODUCTION

All substances, except helium, form a solid phase when they are cooled enough. The vast majority form one or more crystalline phases, where the atoms, molecules or ions pack together to form a regular repeating array (Smart and Moore, 2005). Crystalline solids may take the form of one of the following: (West, 1991).

a. Single crystal that is pure and free from defects,

b. Single crystal which has a modified structure by the creation of defects,

c. Powder (i.e. a large number of small crystals),

d. Polycrystalline solid piece which has a large number of crystals in various orientations in its structure (e.g. a pellet or a ceramic tube).

Each of the aforementioned classes of solids have their own special preparative methods. A vast majority of inorganic solids has been prepared by reacting a solid with another solid, a liquid (melt) or a gas, usually at high temperatures. Since in many reactions with solid compounds, a liquid phase (melt) is formed at the reaction temperature, many 'solid-solid' reactions are actually 'solid-liquid' reactions (Schubert and Hüsing, 2000).

There are numerous ways in order to prepare solid state compounds. So far, alot of methods have been used to synthesize solids. Some of them are co-precipitation, alkali flux methods, electrochemical methods, ceramic methods, the vapor phase transport method, the combustion method and solvo-/hydrothermal method (Raveau and Rao, 1998).

In the present study it is aimed to obtain organic-inorganic hybrid materials, which contain an inorganic framework composed of transition metal (V, W) oxides and organic groups which interact with the inorganic part. In order to achieve this, hydrothermal method, that is a kind of solvothermal technique, is preffered, because traditional solid state syntheses are performed by solid-solid interactions at high temperatures at about 1000°C. Under these conditions thermodynamically stable products are obtained. Moreover, organic molecules will not retain the structural

elements at higher temperatures. Thus, low-temperature techniques, which look like small-molecule chemistry, must be used. As a consequence, hydrothermal synthesis is a powerful method for the preparation of kinetically stable organic-inorganic hybrid materials with the maintenance of the structural elements of the reactants in the final products (Zubieta et al., 1999). Therefore, in the subsequent sections, solvothermal synthesis and hydrothermal synthesis, which is a class of solvothermal synthesis, are described.

1.1. Solvothermal Synthesis

Many inorganic phases are unstable under traditional high-temperature solid-state conditions. Thus, methods with mild conditions such as solvothermal processes can be preferred. Solvothermal synthesis occurs in a liquid medium above the boiling point and 1 bar pressure. In this method, different solvents can be used depending on the desired product in the required temperature and pressure (Byrappa and Yoshimura, 2001). Also, in case of that the solubilities are not high enough in one solvent, or the product reacts with the used solvent, other solvents have to be preferred (Schubert and Hüsing, 2000).

1.1.1. Hydrothermal Synthesis

If an aquous solution is used as the reaction medium in solvothermal synthesis, it is named ‘hydrothermal synthesis’. Water is the most important solvothermal reaction medium, however, a lot of nonaquous solvents, such as ammonia, ethanol and methanol, can also be used (Byrappa and Yoshimura, 2001).

1.1.1.1. History of Hydrothermal Synthesis

The hydrothermal technique has been the focus of interest of the scientists and technologists of different disciplines, especially in the last fifteen years. The hydrothermal term is based on geological origin, relating to the natural processes which

occur by the combined action of heat and water under pressure. It was first used by the British Geologist, Sir Roderick Murchison to describe the action of water at elevated temperature and pressure which makes changes in the earth's crust giving rise to the formation of various rocks and minerals (Byrappa and Yoshimura, 2001).

The largest single crystals formed in nature, some of the largest quantities of synthetic single crystals (quartz crystals of 1000 kg) and the majority of minerals are of hydrothermal origin. Mineral formation in nature under elevated pressure and temperature conditions in the presence of water encouraged the scientists to develop the hydrothermal technique.

During World War II, many scientists in Europe and North America were forced to grow large size crystals because of the demand for the large quartz crystals. Barrel synthesized zeolite that did not have a natural counterpart for the first time in 1948 and this opened a new field of science 'molecular sieve technology'. The success in the growth of quartz crystals contributed the demand for hydrothermal crystal growth.

Today, hydrothermal technique is an interdisciplinary technique which draws the attention of scientists and technologists from different branches of science, such as geologists, biologists, physicists, chemists, engineers ceramists, hydrometallurgists and material scientists.

1.1.1.2. Definition of Hydrothermal Synthesis

Despite the fact that hydrothermal method had made a great progress, there is not a total agreement about its definition. The term 'hydrothermal' is generally used to indicate any heterogeneous reaction in the presence of aqueous solvents or mineralizers under high pressure and temperature in order to dissolve and recrystallize materials which are comparatively insoluble under ordinary conditions (Byrappa and Yoshimura, 2001). According to Morey and Niggli, in hydrothermal synthesis the components are subjected to water at temperatures near or above the critical temperature of water (□ 370 °C) in closed bombs. Byrappa (1992) defines hydrothermal synthesis as any heterogenous reaction in an aquous medium that is carried out above room temperature and at pressure greater than 1 atm. Yoshimora (1994) states that, hydrothermal sytnhesis includes reactions occuring under the conditions of high-temperature-high-pressure (

>100 °C, > 1 atm). However the majority of scientists think that hydrothermal synthesis takes place above 100°C temperature and 1 atm pressure, there is not a definite lower limit for temperature and pressure conditions

Under hydrothermal conditions reactants, which are not easily dissolved, go into solutions forming complexes by the action of solvents or mineralizers. Specific physical properties, such as high solvation power, high compressibility and mass transport of these solvents under hydrothermal conditions provide different types of reactions such as the synthesis of new phases, stabilization of new complexes or crystal growth of various inorganic compounds (Byrappa and Yoshimura, 2001).

All of the liquids including water exbihit different properties under hydrothermal conditions, especially at the critical temperature. The critical point, which is shown in Figure 1.1, indicates the end of liquid-vapor coexistence curve at the critical temperature, T_c, and pressure, P_c.

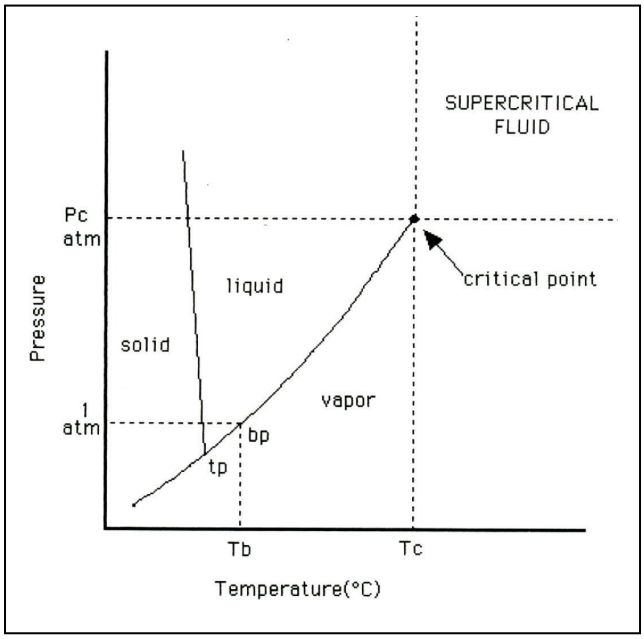

Figure 1.1. Phase diagram of water.
(Source: Schubert and Hüsing, 2000)

Water is defined as supercritical, when it becomes above its critical temperature and pressure. The properties of supercritical water exhibit both the properties of a gas and a liquid which vary depending on the pressure and temperature. As the temperature raises, the liquid becomes less dense as a result of thermal expansion and at the same

time the gas becomes denser. At the critical point both phases have the same densities. The compound is neither liquid nor gas any longer above the critical point, and it becomes supercritical fluid which displays properties between gas and liquid (Figure 1.1).

Conditions between 100 - 150^{o}C and 150 - 375^{o}C are defined as superheated and hydrothermal, respectively. Water under hydrothermal conditions carry the characteristics of supercritical state and it displays significant properties. It can dissolve nonionic covalent compounds (insoluble oxides). At high temperatures and pressures, the viscosity decreases causing the mobility to increase and diffusion processes become easier. The low viscosity and high mobility of supercritical water makes it a very convenient medium for preparing metastable phases and good quality single crystals (Byrappa and Yoshimura, 2001).

Hydrothermal reactions are carried out in closed vessels, thus, the pressure-temperature relations of water at constant volume are significant. In most of the hydrothermal experiments, the pressure is determined by degree of filling and the temperature. A study about the temperature-pressure behaviour of water with different filling ratios was reported by Laudise. If the autoclave is filled less than 32 %, liquid level decreases as temperature rises and gas fills the autoclave at temperatures below the critical temperature (i.e. liquid is lost). When the filling is increased with water, the autoclaves will be filled at lower temperature. Thus, hydrothermal crystallization is performed with degrees of filling of 32% with pressures of 100 bar and more successfully above 65% with pressures of 200 - 3000 bar (Laudise, 1987). Figure 1.2, illustrates the pressure-temperature relations of water for different degrees of filling.

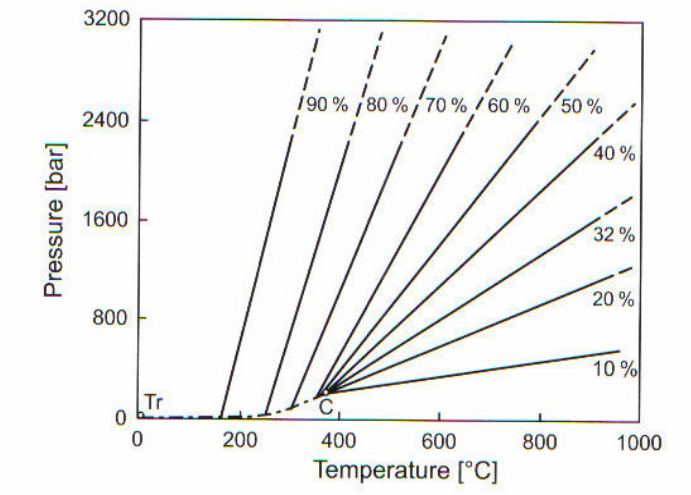

Figure 1.2. Pressure/temperature dependence of water for different degrees of filling of the reaction vessel. (Source: Schubert and Hüsing, 2000)

In hydrothermal synthesis, water acts as the solvent, pressure transmitting medium and sometimes as a reactant. But some compounds do not have enough solubilities in water even at supercritical or near supercritical conditions. Therefore, some small, ionic and soluble compounds called 'mineralizer' can be added to the reaction medium to speed up the crystallization process. A mineralizer increases the solubility of the solute by attacking the starting material (Schubert and Hüsing, 2000). The hydroxides of the alkali metals, silicates, germanates, or elemental metals, alkali salts of weak acids, (e.g. Na_2CO_3, Na_3BO_3, Na_2S), or the chlorides of alkali metals can be used as mineralizers.

A typical hydrothermal procedure is performed like that: The starting materials are put into the reaction vessel and the vessel is filled to the desired degree with the solvent (water and mineralizer). The mixture is heated to the desired reaction temperature. At this temperature the nutrient materials react and/or transform, mainly through dissolution and precipitation to the stable compound. After cooling the autoclave slowly to room temperature, the product is isolated by filtration and washed in order to obtain the pure product (Schubert and Hüsing, 2000).

1.2. Organic-Inorganic Hybrid Materials

Hybrid material is a material, that contains two moieties combined on the molecular scale. Organic-inorganic hybrid materials are formed by the association of organic and inorganic components (Mutin et al., 2003). Hybrid compounds can involve a wide range of molecules for both inorganic and organic parts. Inorganic components generally include transition-metal oxides and p-block elements and organic components involve mostly organoamine ligands. By combining these two moieties, a new material can be obtained which have different and developed properties. Altough metal oxides display spesific properties and have a lot of applications, generally there is a correlation between the complexity of the structure and its functionality. Thus, the design and synthesis of organic-inorganic hybrid materials is contemporary interest (Zubieta et al., 1999).

Many of the naturally occuring oxides include mixtures of inorganic oxides which coexist with organic molecules. The organic components can dramatically influence the microstructures of inorganic oxides by controlling the nucleation and the growth of the inorganic oxide framework. There is a synergistic interaction between the organic and inorganic components. This interaction allows the structural information from the organic molecule to the inorganic scaffold. Also there is a shift from thermodynamic to kinetic domain, thus structurally more complex phases can be obtained instead of equilibrium phases (Zubieta et al., 1999).

Hydrothermal synthesis is a favourable method for preparation of organic-inorganic hybrid materials because the structural elements of the reactants are retained in the final products.

In organic-inorganic hybrid compounds, organic components can serve as charge compensating groups, space-filling units, structure directing agents, templates, tethers between functional groups, or conventional ligands as illustrated in Figure 1.3 (Zubieta et al., 1999).

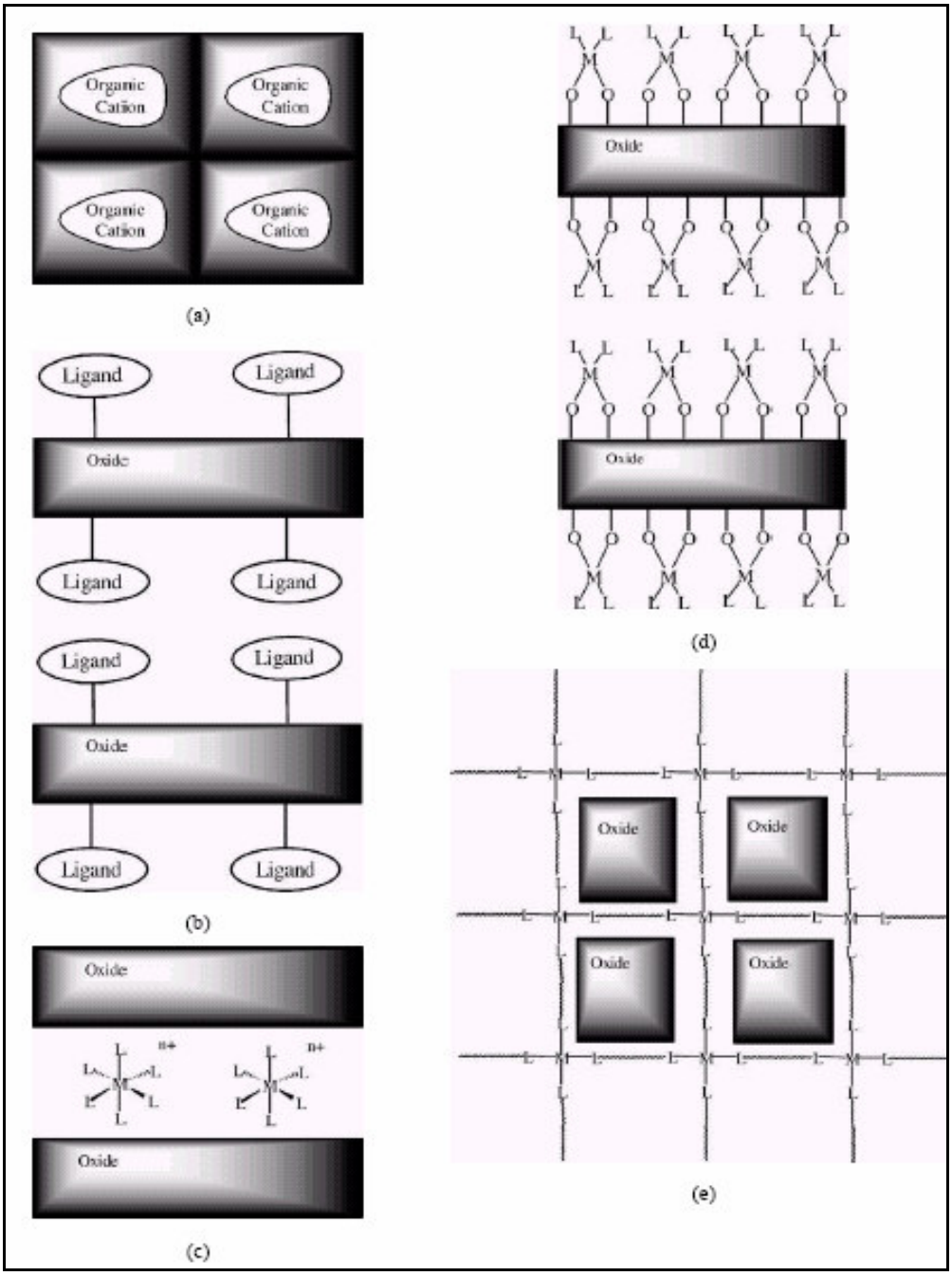

Figure 1.3. Schematic representations of various modes for involvement of organonitrogen components in molybdenum oxide materials. (Source: Hagrman et al., 2001)

Organic ligands can act as charge compensating ligands. They occupy the spaces in the porous structures such as zeolites, mesoporous oxides and transition metal containing phosphates (Figure 1.4.).

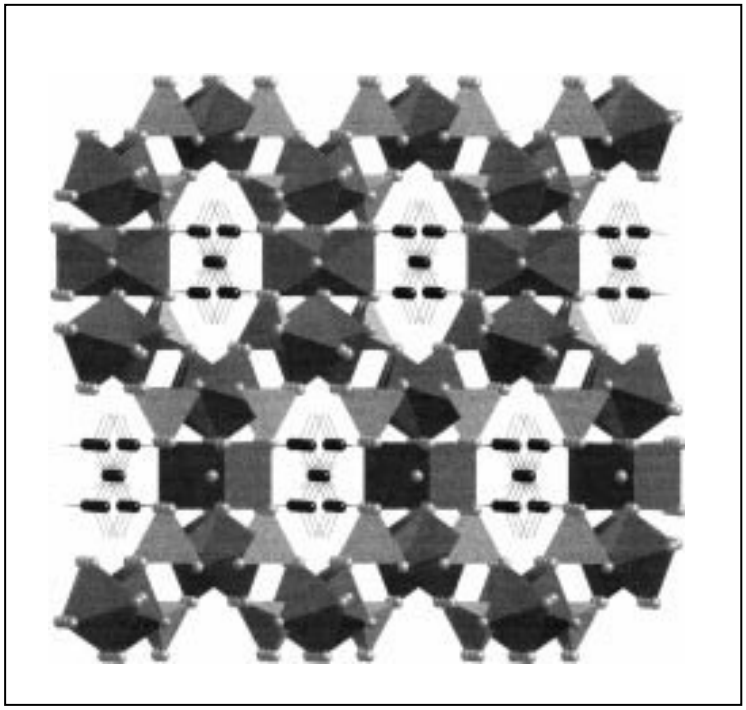

Figure 1.4. A polyhedral representation of the V-P-O framework of $[H_3N(CH_2)_3NH_3]$ $[(VO)_3(OH)_2(H_2O)_2(PO_4)_2]$ down the crystallographic a axis. (black polyhedra: vanadium oxides, gray polyhedra: phosphates) (Source: Zubieta et al., 1999)

As illustrated in Figure 1.4, ammonium cations occupy the channels of the V-P-O framework. Hydrogen bondings exist between the NH groups of the cation and the oxygen atoms of the framework.

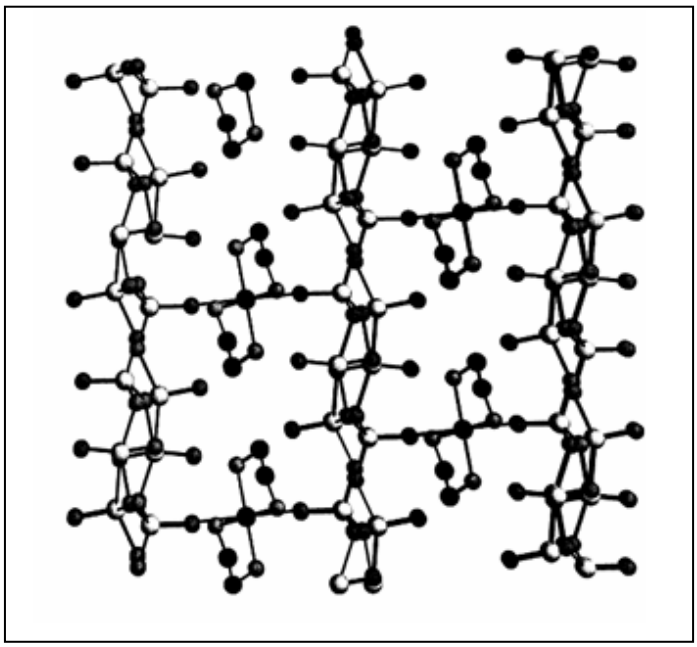

Figure 1.5. View of $Cu(en)_2[V_6O_{14}]$ structure showing $Cu(en)_2$ between the layers. (black spheres: oxygen, white spheres: vanadium) (Source: Ollivier et al., 1998)

Figure 1.5, shows the interlamellar view of the compound $Cu(en)_2[V_6O_{14}]$. The structure is based on vanadium oxide framework and the ethylenediamine ligands which are coordinated to the secondary metal ion Cu(II). $[Cu(en)_2]^{2+}$ complexes exist between vanadium oxide single-layers.

In this study, the focus of interest was the hydrothermal synthesis of organic-inorganic hybrid materials considering the structural diversity, unusual properties and applications of organic-inorganic hybrid compounds. Therefore, hydrothermal technique was preferred in order to obtain novel structures with retention of the organic components owing to the mild conditions of this technique.

CHAPTER 2

EXPERIMENTAL METHOD

2.1. Reaction Autoclaves

Hydrothermal reactions are carried out in closed vessels called 'autoclave'. An ideal hydrothermal autoclave should meet the following characteristics (Byrappa and Yoshimura, 2001):

a. Inertness to acids, bases and oxidizing agents.

b. Leak-proof with unlimited capabilities to the required temperature and pressure.

c. Rugged enough to cope with high pressure and temperature experiments for long duration, thus, no machining or treatment is needed after each experiment

In this study, PTFE (polytetrafluoroethylene)-lined acid digestion bombs are used as reaction autoclaves. These are purchased from Parr Instrument Company (Illinois, USA) and Teflon is used as the lining material. Considering that the maximum operating temperature is 250°C and the maximum pressure is 1800 psi, all the experiments are carried out under mild hydrothermal conditions. The autoclave consists of a spring-loaded, broad flanged closure which is sealed by tightening the bomb cap with a hook spanner wrench (Figure 2.1). Teflon, the lining material, has a larger coefficient of thermal expansion versus the material in which it is enclosed. In case of heating and cooling, the Teflon material expands, thus it is useful to maintain a constant pressure on Teflon by a spring-loaded closure (Byrappa and Yoshimura, 2001).

Figure 2.1. Schematic representation of an autoclave with its parts. (Inset shows the Teflon liner) (Source: Kepenekci, 2009)

In the laboratory, 23 mL Teflon lined acid digestion bombs (Parr Instruments, model 4749), shown in Figure 2.1 with all the parts, were used as the reaction autoclaves. Starting materials were added to the Teflon cup and it was placed into the autoclave. Then, the corrosion and the rupture discs were placed on top of the liner and the spring with upper and lower pressure plates was added. Finally, with a screw cap, the bomb was closed and placed into an oven for 1-3 days at temperatures between 170-190°C. After the reaction was finished, the autoclave was allowed to cool to room temperature slowly. Then the product was washed with distilled water and ethanol. The obtained product was firstly observed under the J.P. Selecta Zoom Stereo Microscope. Then, some of the single crystals were selected for further characterization.

2.2. Characterization Techniques

After the synthesis of a solid, it is important to identify the compound by using some characterization techniques. There are a lot of methods to achieve this and these methods vary depending on the nature of the substance. For molecular materials spectroscopic methods and chemical analysis can be used for identification. If the obtained compound is non-molecular and crystalline, it is usually identified by X-ray crystallography and supported by chemical analysis.

2.2.1. Diffraction Techniques

Diffraction techniques are used for fingerprint characterization of crystalline materials and for the determination of their crystal structures (West, 1991).

2.2.1.1. X-ray Powder Diffraction

A completely ground crystalline powder is composed of a lot of small crystals called 'crystallites' which are oriented randomly. If such a substance is put in the path of a monochromatic X-ray beam (Figure 2.2), diffraction takes place from the planes in these crystallites which are oriented at the correct angle to fulfill the Bragg condition ($n\lambda = 2d \sin\theta$). These diffracted beams make an angle of 2θ with the incident beam. The reflections lie on the surface of cones whose semi-apex angles are equal to 2θ since the crystallites can lie in all directions while retaining the Bragg condition. A flat film which is placed in front of the powder sample records a photograph composed of concentric rings (Smart and Moore, 2005).

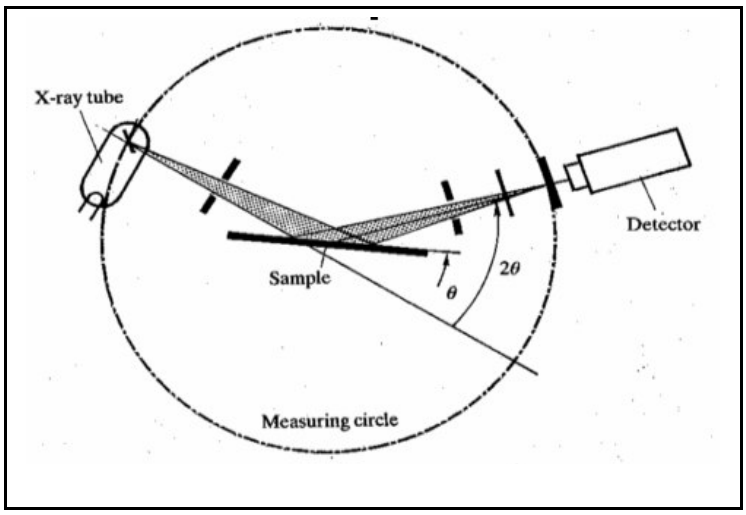

Figure 2.2. The X-ray Spectrometer.
(Source: Smart and Moore, 2005)

An X-ray powder diffraction pattern includes a set of lines or peaks which have different intensities and positions (d-spacing or Bragg angle, θ) as illustrated in Figure 2.3. The line positions are fixed and characteristic for a given compound. However, the intensities can change depending on the method of the sample preparation and the instrumental conditions (West, 1991).

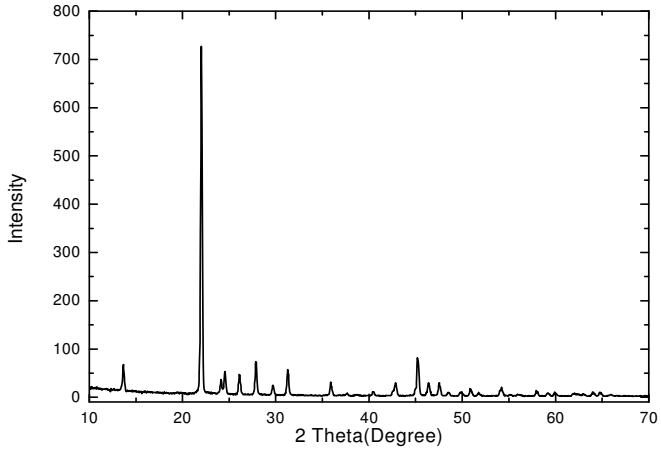

Figure 2.3. Powder X-ray diffraction pattern of $(VO)(H_2PO_4)_2$.

For X-ray powder diffraction analysis of our compounds, Philips X'Pert Pro X-ray Diffractometer was used. The data were collected by using CuKα (λ = 1.5406 Å) radiation at settings of 45 kV and 40 mA for 2θ values of 5° to 70°.

Each crystalline material has its own characteristic powder diffraction pattern. These patterns exist in a regularly updated library known as JCPDS - Joint Committee for Powder Diffraction Standards- file (formerly known as the ASTM File) and this file includes more than 35000 inorganic substances.

2.2.1.2. Single Crystal X-ray Diffraction

In this method, diffraction patterns are collected from one single crystal rather than randomly oriented crystals found in a powder. From a single crystal, the position and intensity of the *hkl* reflections can be measured accurately and from these data the unit cell and space group of the crystal and the precise atomic positions can be determined. This method can be performed with speed and accuracy, and it is one of the most powerful structural techniques to identify the structures of crystals.

Single crystal X-ray diffraction data are collected by using a computer-controlled diffractometer, which measures the Bragg angle (θ), and the intensity (I) for each hkl reflection.

A single crystal is mounted vertically on a goniometer thus it can be rotated about one of the crystallographic axes. The diffraction from each plane will lie on the surface of a set of cones as shown in Figure 2.4. By rotating the crystal, each plane is brought into the diffraction condition. The reflections can be recorded on a film which is wrapped around the rotating crystal. Eventually, the intensity of each reflection is measured. Thus, all the data necessary to solve the crystal structure are obtained (Smart and Moore, 2005).

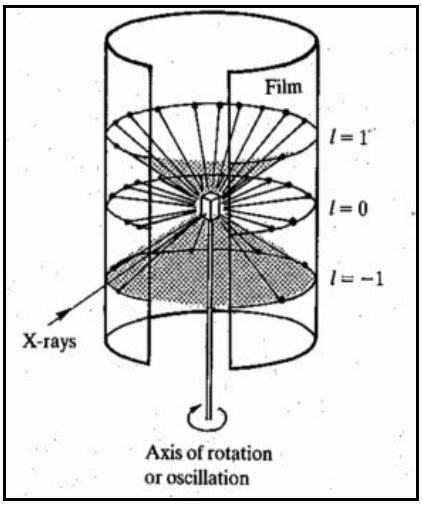

Figure 2.4. Cones of diffracted rays produced by a single crystal.
(Source: Smart and Moore, 2005)

In order to obtain highly precise results from this analysis, it is important to use high-quality single crystals. Therefore, the crystals must have some properties. They must be single without any powder attached to it. They must be in proper size which in 0.1 to 0.6 mm on an edge and a well-defined shape with lustrous faces (Tanaka and Suib, 1999).

2.2.2. Microscopic Techniques

In order to examine a solid, it is usually valuable to look at it under magnification. Because, materials may look different than they visually appear when they are examined under the microscope (West, 1991).

There are many kinds of microscopes and they can be divided into two groups which are optical microscopes and electron microscopes.

Optical microscopes can be used in order to examine particles down to a few micrometers under high magnification. However, for submicrometer-sized particles electron microscopes must be used (West, 1991).

In this study, scanning electron microscope was used in order to examine the surface of the crystals and to get information about their elemental content by the help of the EDX mode.

2.2.2.1. Scanning Electron Microscopy

Electron microscopy is a very useful technique which gives structural information over a wide range of magnification. Scanning electron microscopy (SEM) has a lot of advantages over optical microscopy. The texture, topography and surface features of solid pieces or powders with sizes up to tens of micrometers can be studied with scanning electron microscopy. Because of the depth of focus of SEM instruments, the resulting pictures have a definite three dimensional quality. Also some SEM instruments have the additional property of doing elemental analysis.

The SEM uses electrons instead of light to form an image. Electrons from the electron gun are focused to a small spot on the surface of the sample. The electron beam is scanned systematically over the sample. These bombarding electrons, also named primary electrons, remove the electrons from the specimen itself. When it hits the sample, other electrons (backscattered or secondary) are ejected from the sample. Detectors collect the secondary or backscattered electrons, and convert them to a signal that is sent to a viewing screen similiar to the one in an ordinary television, producing an image. The resolution of SEM is between 100 Å and 10 μm (West, 1991).

2.2.3. Spectroscopic Techniques

There are a lot of different spectroscopic techniques. Actually all of them are based on the same principle. Under certain conditions materials can absorb or emit energy which can take different forms and it is usually electromagnetic radiation (Gün, 2006).

Experimental results or spectra consist of a plot of intensity of absorption or emission (y axis) as a function of energy (x axis). The energy axis is usually expressed with frequency or wavelength.

In our study infrared spectroscopy was usually used in order to comment about the structures by comparing the spectral data of our compounds with the spectral data of the compounds already exist in the literature.

2.2.3.1. Infrared Spectroscopy

Atoms in solid compounds vibrate at frequencies of 10^{12} to 10^{13} Hz. Vibrational modes, which include pairs or groups of bonded atoms, may be excited to higher energy states by absorption of radiation in appropriate frequencies. In the IR technique the frequency of the incident radiation which passes through a thin sample of compound is diverse and the quantity of radiation absorbed or transmitted by the sample is measured (West, 1991). An IR spectrum is the plot of intensity of absorption as a function of frequency or wavenumber.

Inorganic solids tend to give characteristic vibrational spectra, thus the obtained data can be used for identification of unknowns such as covalently bonded hydroxyl groups, trapped water, carbonate, nitrate etc, by using reference spectra (West, 1991).

The IR absorption spectra of single crystals were studied in the range of 4000-400 cm^{-1} by using Perkin-Elmer Spectrum 100 FT-IR spectrometer. Sample preparation was done by preparing pellets by mixing 1-2 mg of sample with 100-150 mg of KBr. The sample-KBr mixture was ground with mortar and pestle and placed inside a die. Then, it was held in a hydraulic press for 5 minutes under 10000 psi pressure. After that, the pellets were placed inside the spectrometer port for the measurements. Samples were run in transmittance mode.

CHAPTER 3

VANADIUM OXIDES

Oxygen is the most abundant element found in land and it is also highly reactive. Thus, there are a lot of oxides for most of the elements, with the exceptions of radon and lighter noble gases. Also there are inorganic oxides ever-present in the geosphere and biosphere. For instance, hydrogen oxide, which is the basis of life, and most ores and gems, bones, teeths and spicules are some of the examples of solid state oxides. Also aluminosilicates, which are the complex compounds of oxygen with silicon and aluminium, exist copiously in igneous rocks.

Inorganic oxides have attracted great interest due to their vast range of structures, compositions and properties that lead to various applications ranging from heavy construction to microelectronic circuitry. Table 3.1, illustrates some of the applications of chosen metal oxides (Zubieta et al., 1999).

Table 3.1. Selected examples and applications of inorganic oxides.
(Source: Hagrman et al., 2001)

Metal class	**Examples**	**Applications**
Oxide sensors	$BaTiO_3$, $PbZrO_3$	Temperature sensors, piezo speakers
Electronic materials	ZnO, $BaTiO_3$	Surge protectors, high T semiconductors
Catalysts	$Bi_2Mo_2O_9$ $(VO)_2P_2O_7$, V_2O_5/TiO_2, $SiO_2–WO_3$	Selective oxidations, polymerization, Oxidative dehydrogenation,
Ion Exchange	NASICON zeolites	Fast ion conductors, detergents
Optical materials	$KTiOPO_4$,$LiNbO_3$	Harmonic generators, frequency mixers, lasers
Construction oxides	CaO	Concrete, trap for desulfurization
High temperature materials	Vitreous silica	1000–1300 ◦C containers

Among inorganic oxides, vanadium oxides are extensively studied because of their remarkable redox, electrochemical, catalytic and magnetic properties. For example, they can be used as secondary cathode materials for advanced lithium batteries. Also, binary vanadium oxides exhibit a metal-insulator transition, therefore, these materials can be used for highly correlated electronic systems.

Vanadium phosphates, similarly to vanadium oxides, have catalytic and magnetic properties. Vanadium phosphate compounds are particularly interesting due to their catalytic behaviour in the mild oxidation of hydrocarbons to molecules of economic interest. For instance, the vanadyl diphosphate $(VO)_2P_2O_7$, is a catalyst capable of transforming directly butane into maleic anhydride. After the discovery of the efficient catalyst $(VO)_2P_2O_7$, a great number of oxovanadium phosphate hydrates have been synthesized during the last decade. Vanadium phosphates have also received great attention for their rich and striking structural chemistry associated with the ability of vanadium to adopt tetrahedral, pyramidal and octahedral coordination geometries in various oxidation states.

In mineral chemistry vanadium adopts three oxidation states; V(III), V(IV) and V(V) and in its phosphate compounds vanadium can take one of these oxidation states (from III toV) and may adopt different coordinations (from 6 to 4) and different environments (octahedral, pyramidal and tetrahedral) that are illustrated in Figure 3.1. (Hagrman et al., 2001).

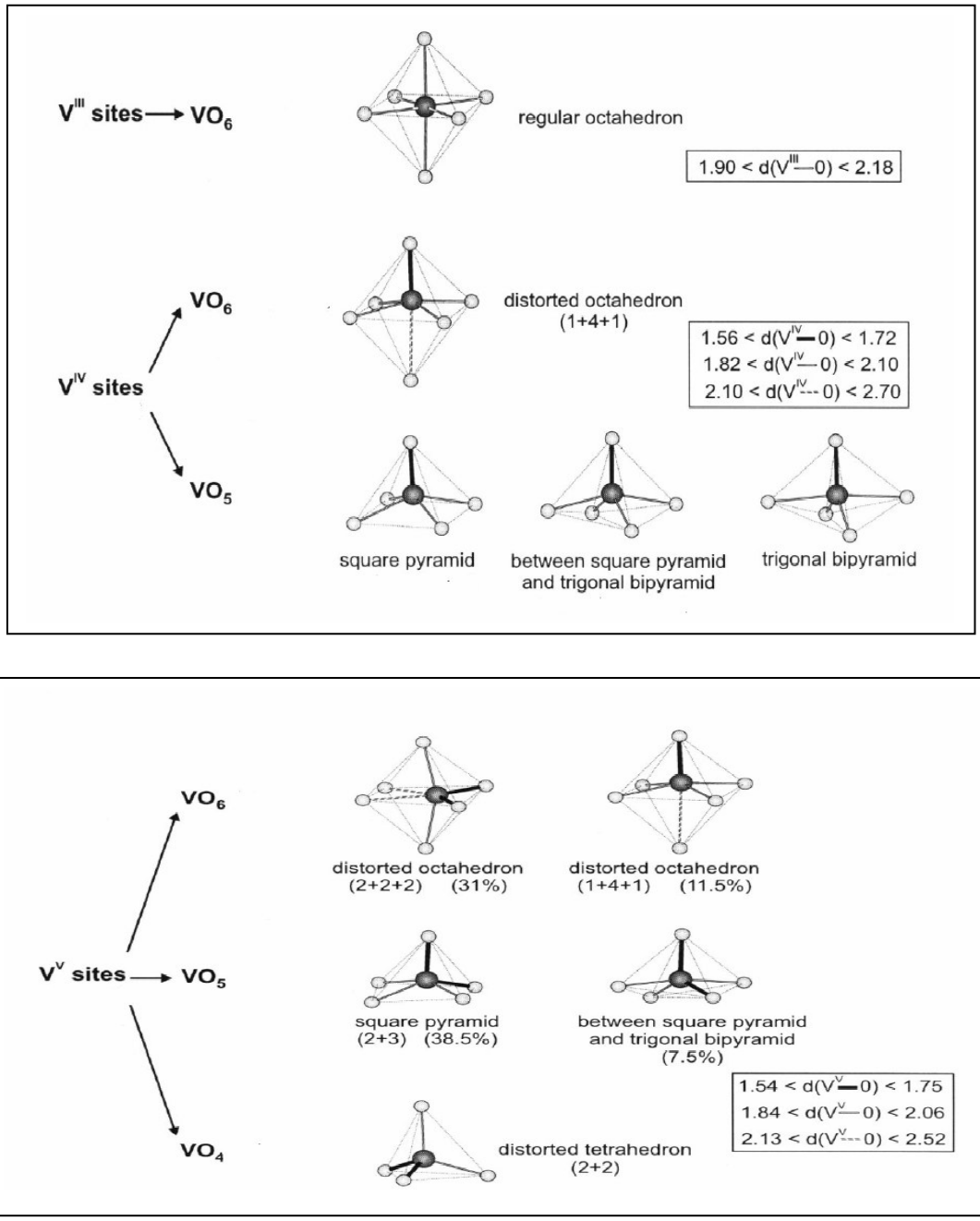

Figure 3.1. Different environments of vanadium encountered in the vanadium phosphates. The V–O distances are given in Å. (Source: Boudin et al., 2000)

The V(III) sites always adopt a regular octahedral coordination and the V-O distances vary from 1.90 to 2.18 Å.

All the V(IV) sites with electronic configuration $3s^2 3p^6 3d^1$ exhibit only five or six coordination with a short V-O bond (from 1.56 to 1.72 Å). Among them, 73.5 % adopt a distorted octahedron. Indicated as (1+4 +1) with a short V-O bond, a distorted octahedron has four intermediate bonds (from 1.82 to 2.10 Å) and a long bond (ranging from 2.10 to 2.70 Å). The other V(IV) sites demonstrate three different five-fold coordination geometries which are square pyramidal, trigonal bipyramidal and the one between these two geometries.

The pentavalent vanadium (V^V) atoms exhibit various geometries such as octahedral, pyramidal and tetrahedral. Most of the V^VO_x polyhedra have two short V-O bonds ranging from 1.84 to 2.06 Å. The longest distances, from 2.13 to 2.52 Å can exist in the V^VO_6 octahedra which can adopt two configurations. One of these structures is described as (2+2+2) with two short, two intermediate and two long V-O bonds and the other geometry denoted as (1+4+1) has one short, four intermediate and one long V-O distances. The VO_5 polyhedra exhibit two short distances and three intermediate ones either in a square pyramidal or in a half square pyramidal-half trigonal bipyramidal geometry. The V^VO_4 tetrahedra always adopt two short V-O distances and two indermediate ones (Boudin at al., 2000).

Figure 3.2, demonstrates the polyhedral representations of some V-P-O structures and cation including vanadium phosphate compounds.

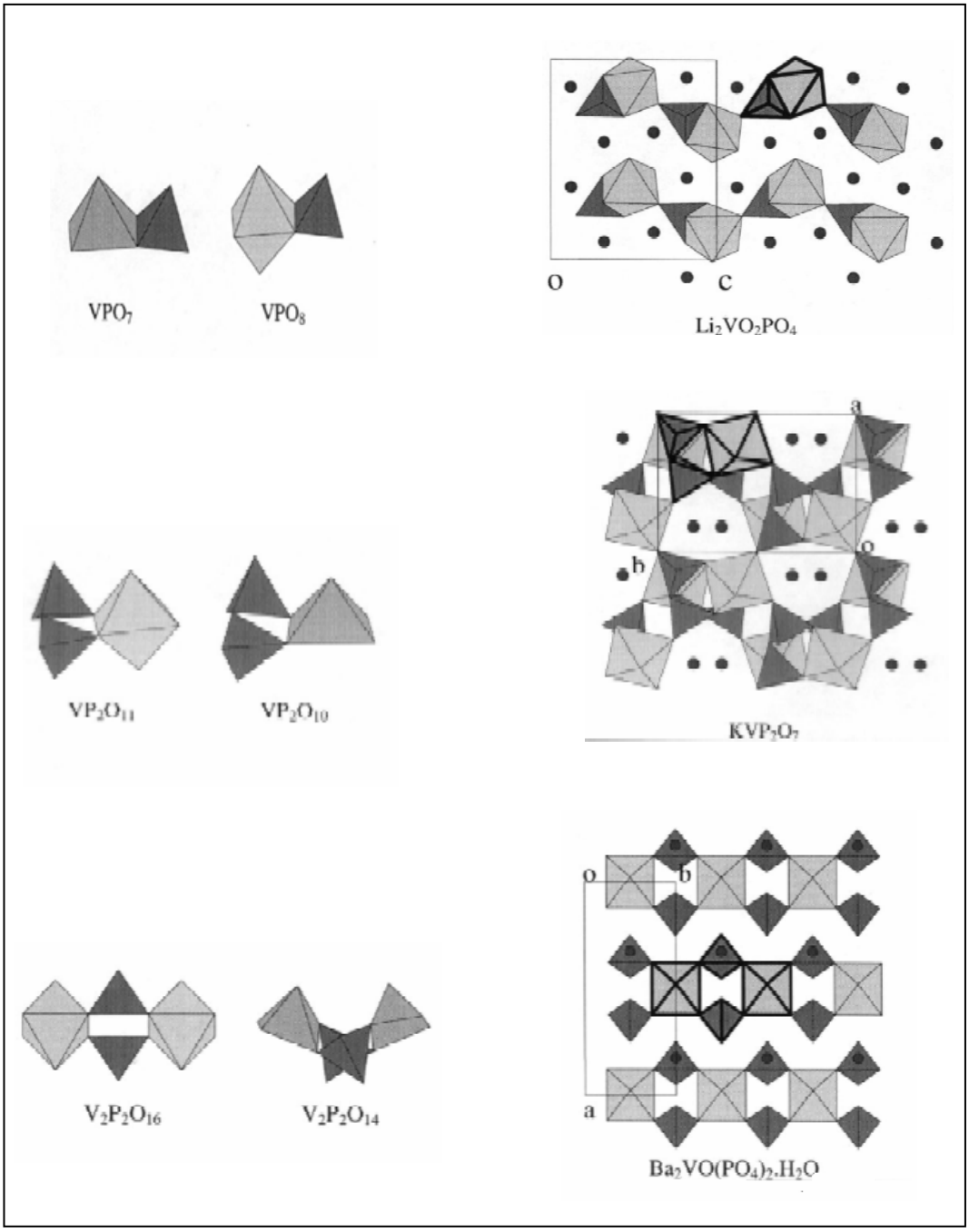

Figure 3.2. The most common mixed units composed of VO_6 and VO_5 polyhedra, which are represented in light and middle grey and the PO_4 tetrahedra in dark grey and examples of AVPO structures in which A represents cations with dark spheres. (Source: Boudin et al., 2000)

3.1. Organic-Inorganic Hybrid Materials Containing Oxovanadium Components

In organic-inorganic hybrid materials, oxovanadium compounds can constitute the inorganic part of the structure and organonitrogen compounds can serve as the organic component. In these hybrid materials, vanadium oxide structures may include either naked $\{VxOy\}^{n-}$ anion or they are often made from vanadate polyhedra combined with other oxyanion tetrahedra such as SiO_4, PO_4, SO_4 and AsO_4 (Hagrman et al., 2001).

As mentioned in the introduction part of this thesis, the organic constituent may adopt a lot of roles such as charge compensating, space-filling, structure directing cation, as a ligand bound directly to the vanadium oxide structure or a ligand bound to a secondary metal site depending on its structure, charge and the presence of a secondary transition or post-transition metal cation besides vanadium component (Zubieta et al., 1999). Therefore, introduction of organic components into oxovanadium containing frameworks give rise to interesting and complicated structures as illustrated in Figures 3.3, 3.4 and 3.5.

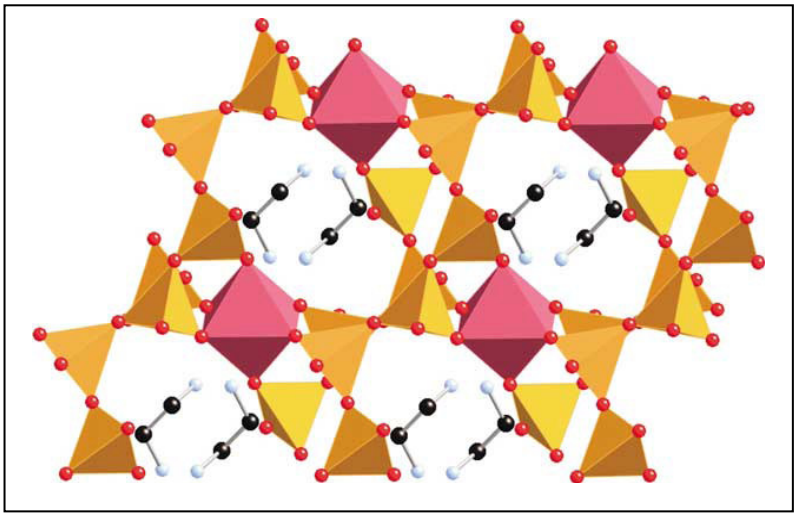

Figure 3.3. Polyhedral representation of the bimetallic layer structure of $(H_2en)_2[MnV_6O_{18}]$, showing the cavities occupied by the cations.(yellow: V(V) tetrahedra, pink: Mn(II) octahedra) (Source: Hagrman et al., 2001)

Figure 3.3 shows an organic-inorganic hybrid material composed of a bimetallic (Mn and V containing) metal oxide scaffold and diprotonated ethylenediamine cations as the organic component which serve as both charge compensating and space filling roles.

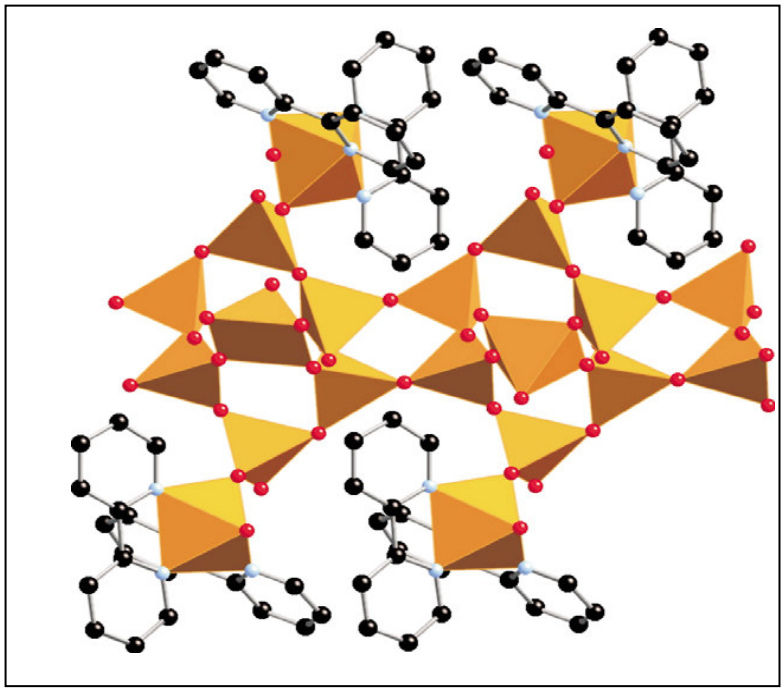

Figure 3.4. Polyhedral representation of $[V_9O_{21}(bpy)_4]$.
(Source: Hagrman et al., 2001)

Figures 3.4 illustrates an organic-inorganic hybrid compound in which the organic components are directly bound to the anionic framework. In Figures 3.5, the organic components are bound to the secondary metal in bimetallic structure denoted as 'MV_xO_y'.

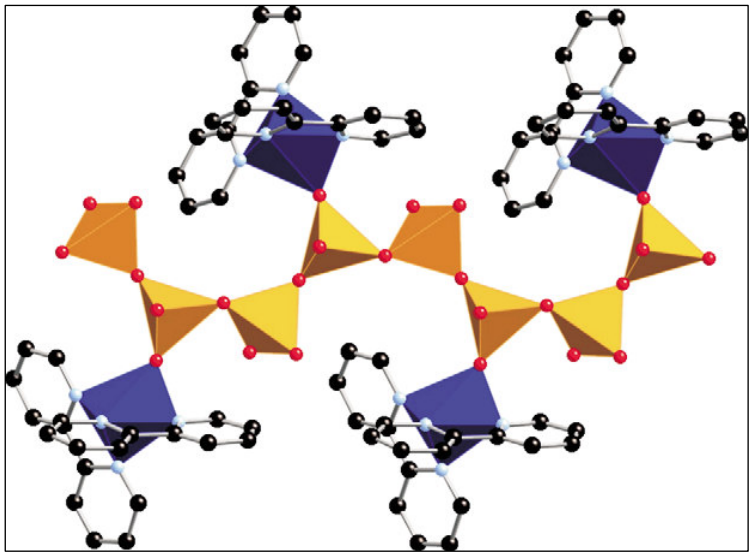

Figure 3.5. Polyhedral view of [Cu(dien)V_2O_6]. (yellow: V(V) tetrahedra, blue: Cu(II) polyhedra) (Source: Hagrman et al., 2001)

3.2. Synthesis and Characterization of Vanadium Compounds

3.2.1. Synthesis and Characterization of $(H_2NC_4H_8NH_2)[(VO)_2(PO_4)_2]$

Green plate-like crystals were obtained from the reaction of $NaVO_3$ (2 mmol, 0.2438 g), V_2O_5 (1 mmol, 0.1818 g), ethylenediamine (1.5 mmol, 0.1 ml), H_3PO_4 (37 mmol, 2.5 ml) and H_2O (278 mmol, 5ml). $NaVO_3$ (Sigma-Aldrich, 98%), V_2O_5 (Riedel-deHaën, 99.5%), ethylenediamine (Merck, 99%) and H_3PO_4 (Sigma-Aldrich, 85%) were used without further purification.

The reaction mixture was loaded into a 23 mL Teflon-lined autoclave and 5 mL of distilled water was added to the mixture to obtain hydrothermal synthesis conditions. The Teflon-lined autoclave was placed into an acid digestion bomb and it was heated at 170 °C for 3 days. After the reaction was finished, the autoclave was slowly cooled to room temperature. The product was washed with distilled water and ethanol and green, plate-like crystals were obtained.

$$NaVO_3 + V_2O_5 + \text{ethylenediamine (en)} + H_3PO_4 + H_2O \xrightarrow[3\ \text{days}]{170\ ^\circ C} \text{green plate-like crystals} \quad (3.1)$$

The SEM/EDX results of the green plate-like crystals are demonstrated in Table 3.2. In accordance with the results, the compound contains vanadium, oxygen, carbon phosphorus and nitrogen elements with the weight percentages.of 35.13%, 24.14%, 19.89%, 16.34% and 4.50% respectively.

Table 3.2. SEM/EDX results of $(H_2NC_4H_8NH_2)[(VO)_2(PO4)_2]$.

Element	Wt %
C	19.89
N	4.50
O	24.14
P	16.34
V	35.13

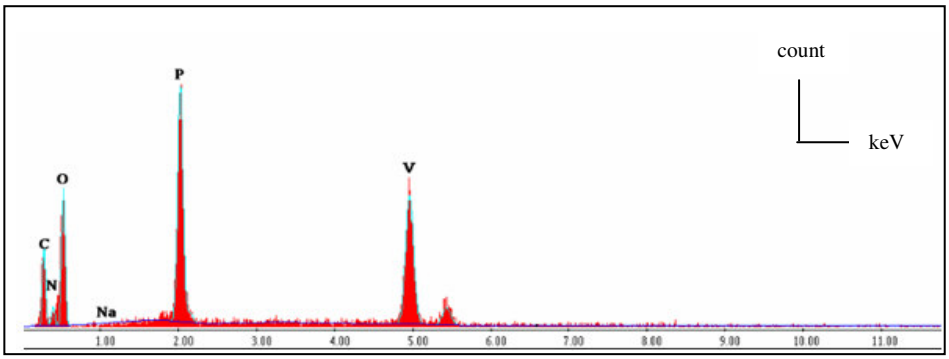

Figure 3.6. SEM/EDX spectrum of $(H_2NC_4H_8NH_2)[(VO)_2(PO_4)_2]$.

The synthesized compound was analyzed by X-ray powder diffraction (XRD) method. The powder pattern of the title compound is demonstrated in Figure 3.7. The powder peaks of the compound did not match well with any of the compounds in the XRD database.

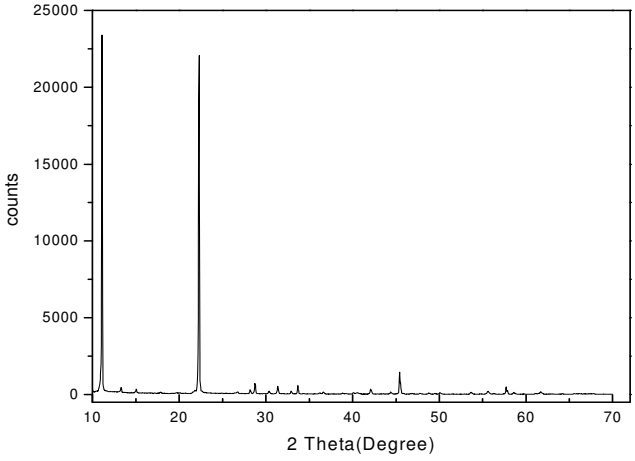

Figure 3.7. Powder pattern of $(H_2NC_4H_8NH_2)[(VO)_2(PO_4)_2]$.

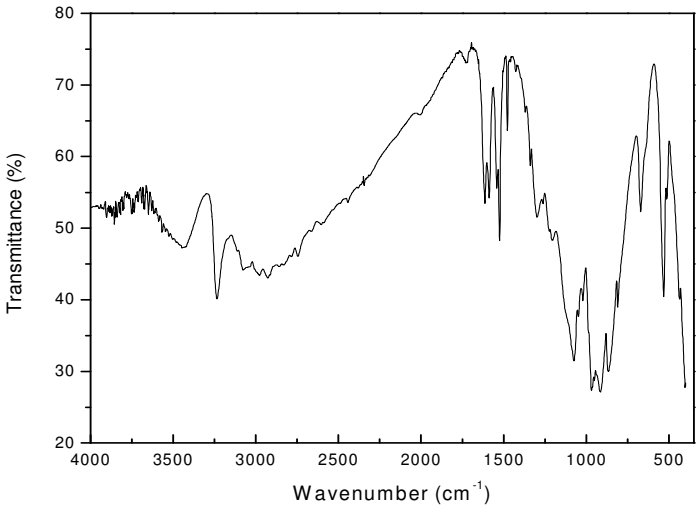

Figure 3.8. FT-IR spectrum of the compound $(H_2NC_4H_8NH_2)[(VO)_2(PO_4)_2]$.

The infrared spectrum of the compound, which is shown in Figure 3.8, was recorded on a Perkin-Elmer Spectrum 100 FT-IR spectrometer with KBr pellets in the 4000–450 cm^{-1} region. Prominent bands can be assigned by comparison with the IR data of related structures. Peaks at 3241 and 3443 cm^{-1} can be attributed to N-H stretching, those in the 1300-1480 cm^{-1} are characteristic peaks of organic groups. The peak at 1082 cm^{-1} can be assigned to P-O stretch. The peaks between 450 and 975 cm^{-1} can be assigned to V=O, terminal V-O or V-O-P vibrations.

3.2.1.1. X-ray Crystallographic Analysis of $(H_2NC_4H_8NH_2)[(VO)_2(PO_4)_2]$

Single crystal X-ray diffraction analysis was done for green, plate-like crystals of $(H_2NC_4H_8NH_2)[(VO)_2(PO_4)_2]$. The structure was solved by direct methods with the program SHELXS (Sheldrick 1997) and by refined full-matrix least-squares techniques with the program SHELXL (Sheldrick 1997) in the Crystal Structure software.

Crystallographic data are given in Table 3.3. Bond lengths (Å) and bond angles (degree) for $(H_2NC_4H_8NH_2)[(VO)_2(PO_4)_2]$ are given in Table 3.4 and Table 3.5 respectively. Final values of the atomic coordinates and isotropic displacement parameters are given in Table 3.6.

Table 3.3. Crystallographic data for $(H_2NC_4H_8NH_2)[(VO)_2(PO_4)_2]$.

Formula	$C_4H_{12}N_2O_{10}P_2V_2$
Formula weight	147.93
Crystal system	Trigonal
Space group	P-*1*
Cell formula units, Z	5
Description	Green plate-like crystals
Unit cell dimensions	a= 6.3345(13) b= 6.3353(13) c= 15.940(3)
Volume ($Å^3$)	639.6(2)

Table 3.4. Bond lengths (Å) for $(H_2NC_4H_8NH_2)[(VO)_2(PO4)_2]$.

V(1)-O(6)	1.499(17)	P(3)–O(7)	1.45(2)
V(1)-O(5)	1.94(2)	P(3)–O(10)	1.52(2)
V(1)-O(3)	1.965(19)	P(3)–O(4)	1.563(17)
V(1)–O(12)	1.990(19)	P(3)–O(5)	1.580(19)
V(1)–O(7)	2.02(2)	P(4)–O(12)	1.499(17)
V(2)–V(1)	1.492(17)	P(4)–O(9)	1.51(2)
V(2)–O(9)	1.96(2)	P(4)–O(3)	1.55(2)
V(2)–O(10)	1.969(19)	P(4)–O(2)	1.555(19)
V(2)–O(4)	1.969(19)	N(1)-C(2)	1.72(13)
V(2)–O(2)	1.973(19)	N(1)–C(1)	2.05(13)
V(2)–O(8)	2.162(19)	C(1)-C(2)	1.31(9)

Table 3.5. Bond angles (°) for $(H_2NC_4H_8NH_2)[(VO)_2(PO4)_2]$.

O(6)- V(1)- O(5)	99.1(9)	O(10)- V(2)- O(2)	89.4(8)
O(6) –V(1) –O(3)	98.2(9)	O(4) –V(2)- O(2)	89.1(8)
O(5) –V(1)- O(3)	89.5(8)	O(1) –V(2)- O(8)	178.9(9)
O(6) –V(1)-O(12)	98.1(8)	O(9) –V(2) –O(8)	83.3(8)
O(5) –V(1)- O(12)	88.7(8)	O(10)- V(2)- O(8)	82.4(8)
O(3) –V(1) –O(12)	163.7(8)	O(4) –V(2) –O(8)	80.6(7)
O(6)- V(1)- O(7)	96.9(9)	O(2) –V(2) –O(8)	80.5(7)
O(5) –V(1) –O(7)	164.0(8)	O(7) –P(3)- O(10)	112.1(11)
O(3) –V(1)- O(7)	88.1(8)	O(7)- P(3)- O(4)	113.3(11)
O(12) –V(1) –(7)	89.2(8)	O(10) –P(3)- O(4)	104.8(10)
O(1) –V(2)- O(9)	97.7(9)	O(7) -P(3)- O(5)	105.6(11)
O(1)- V(2) –O(10)	97.4(8)	O(10) –P(3)- O(5)	111.9(11)
O(9)- V(2)- O(10)	88.1(8)	O(4) –P(3)- O(5)	109.2(9)
O(1) –V(2)- O(4)	99.6(8)	O(12)- P(4)- O(9)	109.7(10)
O(9) –V(2) –O(4)	88.7(9)	O(12)- P(4)- O(3)	105.4(10)
O(10) –V(2) –O(4)	162.9(8)	O(9) –P(4) –O(3)	113.5(11)
O(1)- V(2)- O(2)	98.4(9)	O(12)- P(4)- O(2)	113.2(10)
O(9) –V(2) –O(2)	163.8(8)	O(9)-P(4) –O(2)	105.8(11)
O(10)- V(2)- O(2)	89.4(8)	O(3) –P(4) –O(2)	109.4(10)
O(4) –V(2) –O(2)	89.1(8)	C(2) –N(1)- C(1)	105(5)
O(9) –V(2)- O(4)	88.7(9)	C(2)- C(1) –N(1)	111(7)
O(10) –V(2) –O(4)	162.9(8)	C(1)- C(2)- N(1)	134(8)
O(1) –V(2)- O(2)	98.4(9)		
O(9) –V(2) –O(2)	163.8(8)		

Table 3.6. Atomic coordinates and equivalent isotropic thermal parameters for $(H_2NC_4H_8NH_2)[(VO)_2(PO_4)_2]$.

Atom	x	y	z	Ueq
V1	0.4245(7)	0.0763(7)	0.2903(3)	0.0216(13)
V2	0.9231(7)	0.5762(7)	0.2094(3)	0.0220(13)
P3	0.9257(11)	0.0742(10)	0.2501(4)	0.0193(16)
P4	1.4249(11)	0.5764(10)	0.2500(4)	0.0182(15)
O1	0.925(3)	0.579(3)	0.3030(10)	0.020(4)
O2	1.231(3)	0.579(3)	0.1902(11)	0.021(4)
O3	1.417(3)	0.770(3)	0.3090(12)	0.027(4)
O4	0.919(3)	0.269(3)	0.1901(11	0.025(4)
O5	0.727(3)	0.078(3)	0.3101(11)	0.023(4)
O6	0.425(3)	0.074(2)	0.1963(10)	0.020(4)
O7	1.108(3)	0.075(3)	0.3050(12)	0.031(4)
O9	1.616(3)	0.575(3)	0.1939(12)	0.029(4)
O10	0.921(3)	-0.116(3)	0.1921(12)	0.028(4)
O12	1.427(3)	0.388(3)	0.3067(11)	0.024(4)
O8	0.927(3)	0.574(3)	0.0738(12)	0.028(4)
N1	1.165(17)	0.356(17)	0.436(6)	0.20(3)
C1	1.118(12)	0.743(11)	0.516(4)	0.11(2)
C2	0.772(12)	0.418(11)	0.510(4)	0.11(2)

3.2.1.2. Results and Discussion for $(H_2NC_4H_8NH_2)[(VO)_2(PO_4)_2]$

The novel compound $(H_2NC_4H_8NH_2)[(VO)_2(PO_4)_2]$ was obtained hydrothermally as green plate-like crystals from the reaction of $NaVO_3$, V_2O_5, ethylenediamine (en) and H_3PO_4.

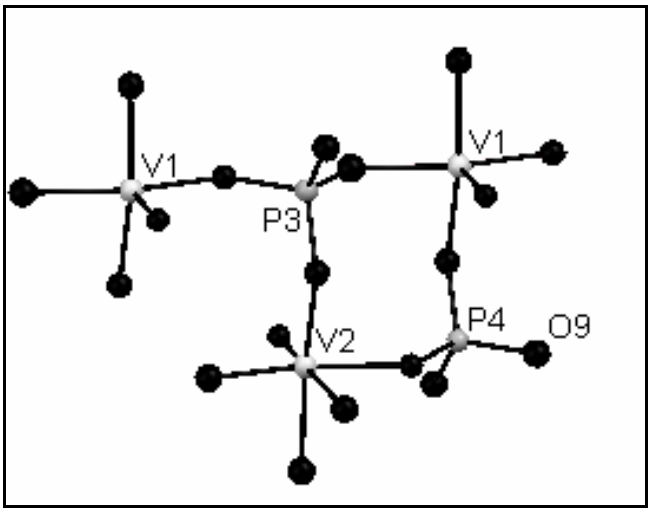

Figure 3.9. The view of coordination in $[(VO)_2(PO_4)_2]^{2-}$ anion.

Figure 3.9, illustrates the coordination environments of vanadium and phosphorus atoms in $[(VO)_2(PO_4)_2]^{2-}$ anion. The whole compound is an extended two-dimensional structure composed of layers of VO_6 octahedra, VO_5 square-pyramids and PO_4 tetrahedra. Vanadyl, (VO^{2+}), moieties are connected through PO_4^{3-} ions and this type of connection generates paralles to crystallographic ab plane resulting in a layered structure as illustrated in Figure 3.10. Organic molecules, the protonated piperazine groups, exist between distinct layers.

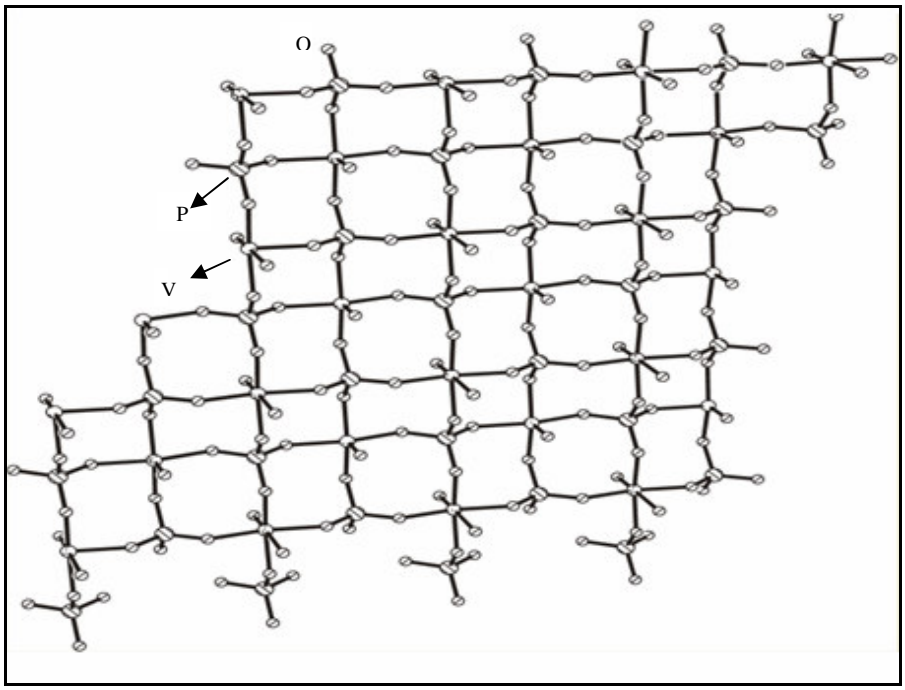

Figure 3.10. View of $(VO)_2(PO_4)_2$ layer.

In VO_6 octahedra there are two types of bond distances between vanadium and oxygen atoms, which are consistent with the values in the literature. First one is V-O long bond distance ranging from 1.96(2) to 2.162(19) Å and the other one is the short bond, 1.492(17) Å, which is consistent with a V=O double bond. The O-V(2)-O bond angles range from 89.2(8) to 178.9(9)°. The bond distances between vanadium and oxygen in square pyramidal geometry are also similar. The long bond distances range from 1.94(2) to 2.02(2) Å and the short V=O bond is 1.499(17) Å. The O-V(1)-O bond angles vary from 99.1(9) to 164.0(8)°. All of the phosphorus atoms are tetrahedrally coordinated to oxygen atoms with the bond distances ranging from 1.45(2) to 1.58(19) Å.

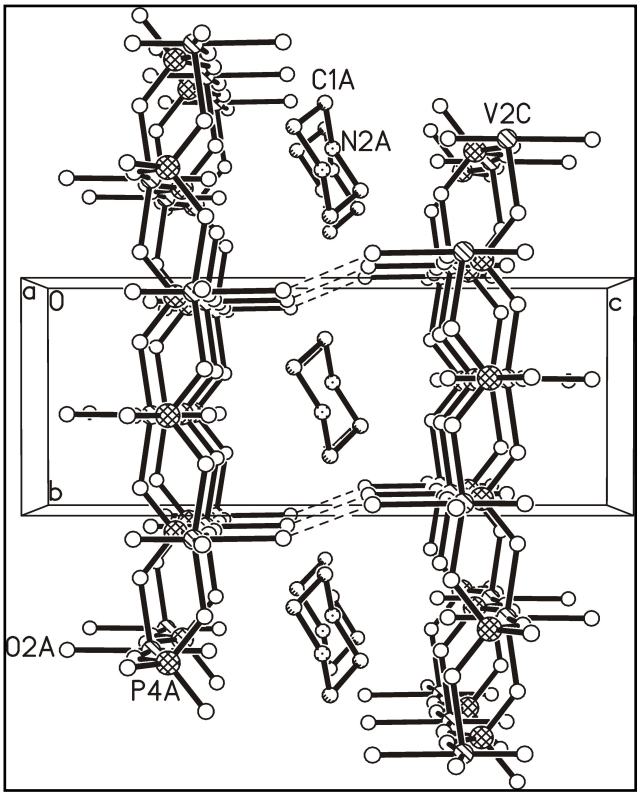

Figure 3.11. Unit cell view of $(H_2NC_4H_8NH_2)[(VO)_2(PO_4)_2]$ from b axis.

The unit cell of the structure (Figure 3.11) is composed of two layers and a diprotonated piperazine ion between these layers. Free diprotonated piperazine cations interact with the oxygen atoms in the inorganic network through N-H…O hydrogen bonds. The distance between two layers is approximately 7 Å.

It can be said that extensive hydrogen-bonding interactions between the organic cations and the inorganic framework play an important role in stabilizing the 3D structure.

It is noteworthy to draw attention to the existence of piperazine molecules instead of expected ethylenediamine molecules between the inorganic layers because of using ethylenediamine as the organic ligand in the synthesis of the title compound. But under hydrothermal conditions, at temperatures higher than 150°C, in closed vessels, it is probable to obtain piperazine from ethylenediamine considering the experiments in the literature to achieve this (Martin and Martell, 1948).

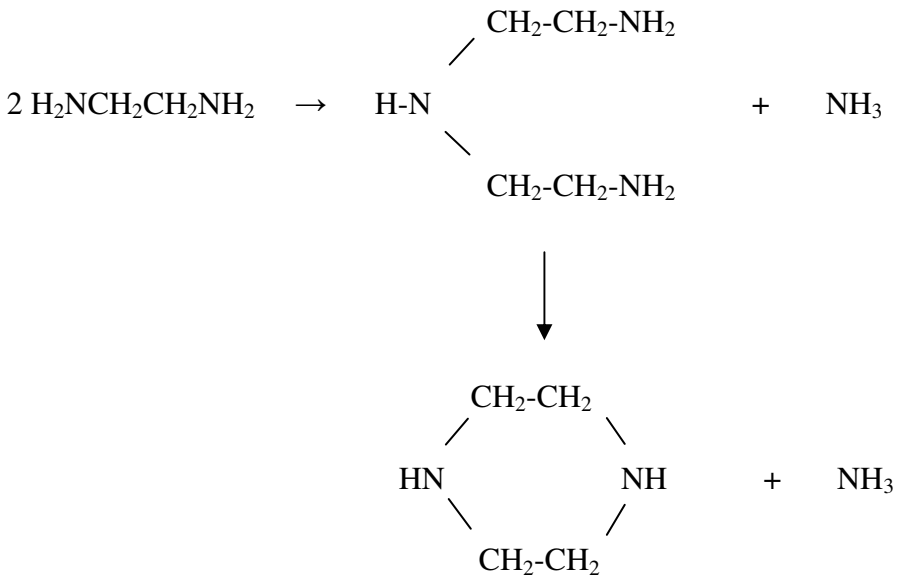

(3.2)

The formation of piperazine from ethylenediamine is thought to be resulted through preliminary formation of diethylenetriamine which then condensed to form piperazine as in the equation.

3.2.2. Synthesis and Characterization of $(VO)(H_2PO_4)_2$

The reaction of $NaVO_3$ (2 mmol, 0.2438 g), ethylenediamine (1.5 mmol, 0.1 ml), H_3PO_4 (52 mmol, 3.5 ml) and H_2O (280 mmol, 5 mmol) yielded blue, rod-like single crystals of $(VO)(H_2PO_4)_2$. $NaVO_3$ (Sigma-Aldrich, 98%), ethylenediamine (Merck, 99%) and H_3PO_4 (Sigma-Aldrich, 85%) were used without further purification.

The reaction mixture was loaded in a 23 ml Teflon-lined acid digestion bomb and heated at 170°C for 3 days. After the reaction was finished, the bomb was cooled slowly to room temperature and the crytals were filtered, washed with pure water and ethanol and then air-dried. Blue, rod-like crytals, as demonstrated in Figure 3.12, were obtained.

$$NaVO_3 + \text{ethylenediamine(en)} + H_3PO_4 + H_2O \xrightarrow[3\ \text{days}]{170^\circ C} (VO)(H_2PO_4)_2 \quad (3.3)$$

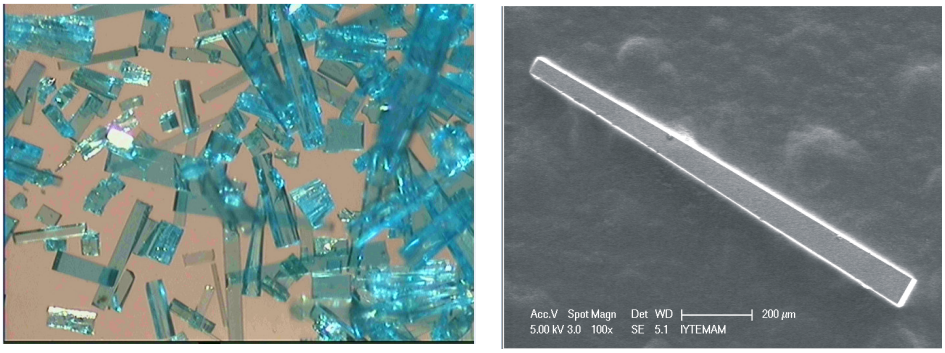

Figure 3.12. Optical microscope and SEM images of $(VO)(H_2PO_4)_2$.

In conformity with the SEM/EDX results of the blue rod-like crystals shown in Table 3.7, the obtained product contains oxygen, phosphorus, vanadium, carbon and nitrogen elements in the weight percentages of 36.76% , 27.23%, 25.76%, 5.07% and 4.99% respectively.

Table 3.7. SEM/EDX results of $(VO)(H_2PO_4)_2$.

Element	Wt%
C	5.07
N	4.99
O	36.76
P	27.23
V	25.76

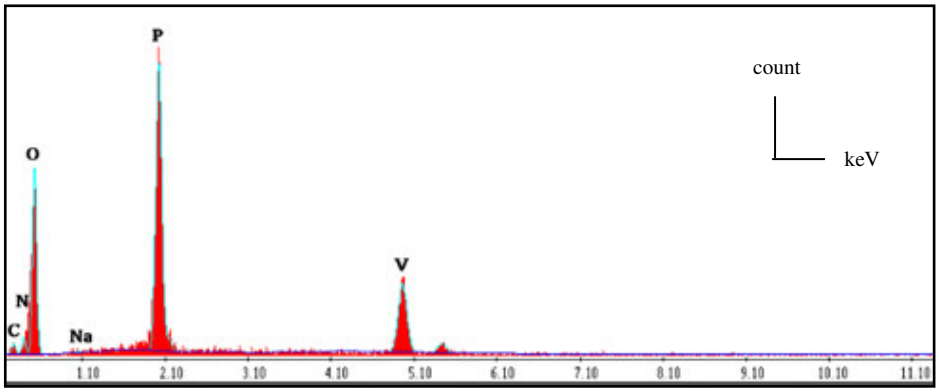

Figure 3.13. SEM/EDX spectrum of $(VO)(H_2PO_4)_2$.

Figure 3.14. shows the powder pattern of the title compound. The powder peaks of the synthesized compound did not match well with the powder patterns of any of the compounds in the XRD database. However, the structure was solved by using the single crystal X-ray diffraction data and it was found to be the known compound $(VO)(H_2PO_4)_2$.

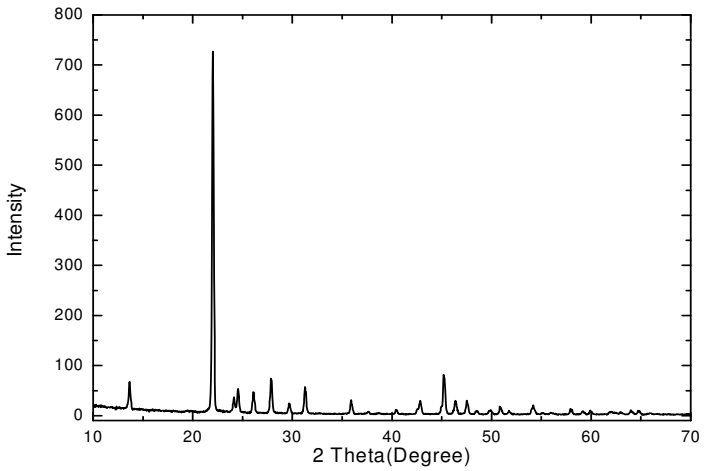

Figure 3.14. Powder pattern of $(VO)(H_2PO_4)_2$.

3.2.2.1. X-ray Crystallographic Analysis of $(VO)(H_2PO_4)_2$

Single crystal X-ray diffraction analysis was done for blue, rod-like crystals of $(VO)(H_2PO_4)_2$. The structure was solved by direct methods with the program SHELXS (Sheldrick 1997) and by refined full-matrix least-squares techniques with the program SHELXL (Sheldrick 1997) in the Crystal Structure software. Crystallographic data are given in Table 3.8.

Table 3.8. Crystallographic data for $(VO)(H_2PO_4)_2$.

Formula	$H_4O_9P_2V$
Formula weight	260.91
Crystal system	Tetragonal
Space group	P*4/ncc*
Cell formula units, Z	4
Description	Blue rod-like crystals
Unit cell dimensions	a=8.9633(13)
	b= 8.9633(13)
	c=7.9151(16)
Volume ($Å^3$)	635.91(18)

3.2.2.2. Results and Discussion for $(VO)(H_2PO_4)_2$

The layered oxovanadium(IV) dihydrogen phosphate, $(VO)(H_2PO_4)_2$ compound, was synthesized hydrothermally and blue rod-like crystals were obtained.

The title compound $(VO)(H_2PO_4)_2$ has a layered two dimensional structure without any organic groups between the layers. The structure consists of VO_5 square pyramids and H_2PO_4 tetrahedra each in turn connecting two adjacent distorted VO_5 pyramids to form a two-dimensional layer parallel to the ab plane. Each VO_5 shares its equatorial O atoms with four H_2PO_4 tetrahedra.

There are two types of bond distances between vanadium and oxygen atoms. One of them is V=O short bond 1.600(7) Å and the other bonds are longer V-O bonds having distances 1.978(3) and 2.357(7) Å. The P-O bond distances vary from 1.501(3) to 1.579(2) Å. The relatively long P-O bonds, 1.579(2) Å, point out the P-OH groups. The O-V-O bond angles range from 79.42(6) to 180.0(1) °.

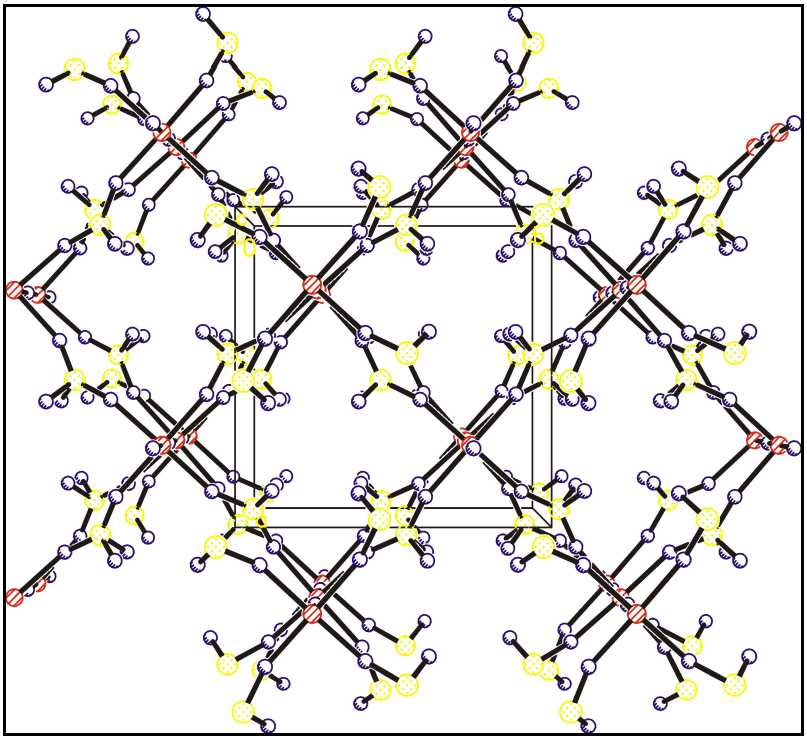

Figure 3.15. Unit cell view of $(VO)(H_2PO_4)_2$ from c axis (yellow: phosphorus, red: vanadium, white : oxygen).

The unit cell of $(VO)(H_2PO_4)_2$, shown in Figure 3.14, is composed of two parallel layers. The two dimensional parallel layers which are extended along the ab plane are separated by ca. 3.99 Å.

The title compound $(VO)(H_2PO_4)$, was studied by some of the scientists in different times. It was synthesized by Hutchings et al. in polycrystalline form and then by Sen et al. as needle-shaped single crystals from the hydrothermal reaction of ammonium metavanadate (0.12 g, 1 mmol) with large excess orthophosphoric acid (3.2 mL, 55 mmol) in the presence of ethylenediamine (0.36 g, 6 mmol) in 20 mL of distilled water in a 250 mL Teflon-lined autoclave for 3 days at 160 °C (Sen et al., 2008).

CHAPTER 4

POLYOXOMETALATES

Polyoxometalates are metal-oxygen clusters formed by early transition metals of groups V and VI (V, Nb, Ta, Mo and W) in their highest oxidation states. (e.g.V^{5+} ,W^{6+}). The chemistry of polyoxometalates started with Berzelius in 1826 with the discovery of dodecamolybdophosphate ion denoted as $[PMo_{12}O_{40}]^{3-}$. However, it is still an area attracting extensive interest, owing to the wide range of their topological properties and great potential applications in various areas such as catalysis, photochemistry, magnetism, and medicine (Kozhevnikov, 2002).

There are lots of different structures of polyoxometalates due to the ability of these compounds to contain heteroatoms with the exception of rare gases. They can be divided into two general groups (Borrás-Almenar et al., 2003).

a. Isopoly anions $[M_mO_y]^{p-}$; which contain Mo, W, or V in its maximum oxidation states.

b. Heteropoly anions $[X_xM_mO_y]^{q-}$ ($x \leq m$); that contain at least one d- or p- block element as the heteroatom such as B, Si, Ge, P, As, Sb, Te, I.

M is called the 'addenda atom' which is the primary constituent of the structure and X is the heteroatom. Addenda atoms constitute the essential part of the building blocks by occupying a metal-oxygen polyhedron MO_x. The most commonly used addenda atoms are molybdenum and tungsten followed by vanadium and niobium which are not very often used. Molybdenum(VI) and tungsten(VI) are the best polyoxometalate formers owing to their favorable combination of ionic radius and charge, and the convenience of empty d orbitals for metal-oxygen π bonding. Sometimes polyoxometalates can include mixtures of these elements in their highest oxidation states. Nearly all the elements in periodic table may serve as heteroatoms in heteropoly anions and the mostly used ones are P(5+), As(5+), Si(4+), Ge(4+), B(3+), etc (Kozhevnikov, 2002).

4.1. Structures of Polyoxometalates

Numerous structural types and stoichiometries of polyoxometalates are known until today and the minimum degree of condensation of addenda atoms are thought to be in the range of 2-6 and the maximum can be as high as a few hundred. According to Pope and Muller, polyoxometalate structures start from a few highly symmetrical basic polyanions and a lot of polyoxometalate structures can be considered as their derivatives. Thus, there are three main structures with a tetrahedron, an octahedron and an icosahedron as their central polyhedron XO_n (n= 4, 6 or 12), which determines the symmetry of the whole polyanion. These structures are known with special names such as Keggin structure with Td symmetry, Anderson-Evans structure in Oh symmetry and Dexter-Silverton polyanion with Ih symmetry (Kozhevnikov, 2002).

The first described and best-known structure is the Keggin structure with the formula $[XM_{12}O_{40}]^{n-}$ (Figure 4.1). Here X is the heteroatom and M is the addenda atom which is generally W^{6+} or Mo^{6+}. The Keggin structure is composed of a central tetrahedron XO_4 and 12 edge- and corner-sharing metal-oxygen octahedra MO_6, which surround this tetrahedron as illustrated in Figure 4.1.

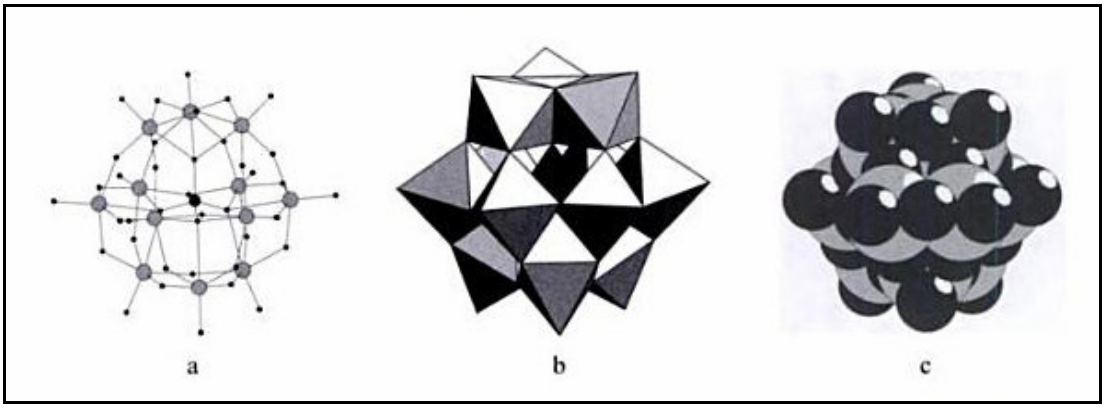

Figure 4.1. a) Bond b) Polyhedral c) Space-filling representations of Keggin polyanion. (Source: Kozhevnikov, 2002)

There are some derivatives of the Keggin structure. One of them is the mostly encountered Wells-Dawson structure, which is a dimeric heteropolyanion formulated by $[X_2M_{18}O_{62}]^{m-}$ where M=Mo^{6+} or $W^{6+,}$ X=P^{5+} or As^{5+} (Kozhevnikov, 2002). Figure 4.2 illustrates the polyhedral view of Wells-Dawson Structure.

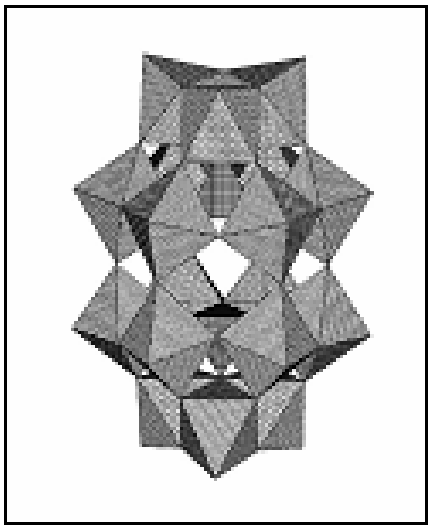

Figure 4.2. Polyhedral representation of the Wells-Dawson Structure.
(Source: Li et al., 2006)

4.2. Polyoxometalate Based Organic-Inorganic Hybrid Materials

Polyoxometalates (POMs) are good candidates for constructing organic-inorganic hybrid materials. They act as the inorganic building blocks of these supramolecular structures. They can lead to forming extended organic-inorganic hybrid materials by means of some interactions such as hydrogen-bonding, van der Waals interactions or weak electrostatic interactions. Hydrogen bonding is the most important one among all. POMs have spherical surfaces which provide the opportunity of forming hydrogen bonding interactions due to having terminal and bridging oxygen atoms which are good hydrogen bond acceptors. Especially, Keggin polyanions are ideal building blocks for making organic-inorganic hybrid materials because of their diverse coordination styles via terminal and bridging oxygens and suitable size (Yang et al., 2010). Figure 4.3, represents an example structure based on Keggin polyanion.

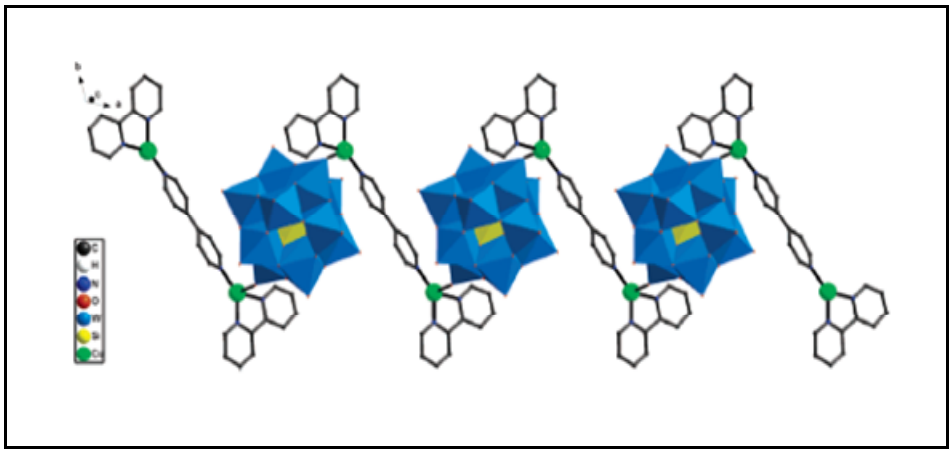

Figure 4.3. Polyhedral and ball-stick representation of the 1D organic-inorganic hybrid zigzag chains in compound $[Cu^{I}(2,2'\text{-bipy})(4,4'\text{-bipy})_{0.5}]_2[Cu^{I}(4,4'\text{bipy})]_2[SiW_{12}O_{40}]$.(blue: W, green: Cu, yellow:Si). (Source: Jin et al., 2006)

Polyoxometalates (POMs) are also significant for displaying extensive self-assembly properties. This gives the opportunity of obtaining multi-dimensional structures. POM-based supramolecular compounds have been studied in many areas such as non-linear optical materials, catalysis, medicine, crystal synthesis and new functional materials (Yang et al., 2010).

In the present study, we aimed to obtain POM-based organic-inorganic hybrid materials because of their intriguing structures and various applications as aforementioned. Therefore, many experiments were performed. The hydrothermal synthesis technique in combination with organic substances yielded significant structures. In this thesis three compounds of tungsten were discussed.

4.2.1. Synthesis and Characterization of Tungsten Compounds

4.2.1.1. Synthesis and Characterization of Novel $(4,4'bipy)_3[HPW_{12}O_{39}]$ and $[Cu(4,4'\text{-}bipy)_4][HPW_{12}O_{40}]$

Single crystals of $(4,4'\text{-}bipy)_3[HPW_{12}O_{39}]$ and $[Cu(4,4'\text{-}bipy)_4][HPW_{12}O_{40}]$ were obtained from the reaction of $Na_6[H_2W_{12}O_{40}]$ (sodium polytungstate) (0.1 mmol, 0.2984 g), $CuCl_2.2H_2O$ (0.5 mmol, 0.0855 g), 4,4'- bipyridine (0.5 mmol ,0.0782 g), H_3PO_4 (0.30 mmol, 0.02ml) and H_2O (390 mmol, 7 ml). $Na_6[H_2W_{12}O_{40}]$ (Alfa Aesar, 99 %), $CuCl_2.2H_2O$ (Merck, 99%), 4,4'- bipyridine (Alfa Aesar, 98%) and H_3PO_4 (Sigma-Aldrich, 85%) were used without purification.

The reaction mixture was stirred in a 23 ml Teflon vessel for an hour in air and the pH value of the mixture was measured to be 2.3 with a pH-meter. Then the 23 ml Teflon-lined autoclave was put into an oven and kept at 170 °C for 3 days. After the reaction was finished, the autoclave was cooled to room temperature slowly. The product was filtered, washed with ethanol and distilled water and then air-dried. Purple, plate-like crystals and green, rod-like crystals were obtained.

$$Na_6[H_2W_{12}O_{40}] + CuCl_2.2H_2O + 4,4'\text{ bipyridine} + H_3PO_4 + H2O$$

$$\xrightarrow[170\ ^\circ C]{3\ days}$$

$$(4,4'\text{-}bipy)_3[HPW_{12}O_{39}] \quad \text{and} \quad [Cu(4,4'\text{-}bipy)_4][HPW_{12}O_{40}] \qquad (4.1)$$

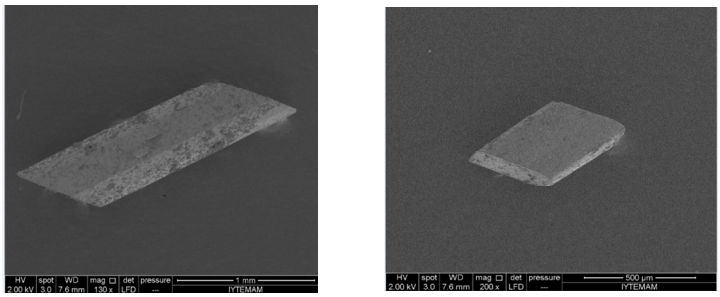

Figure 4.4. Sem images of (4,4'-bipy)$_3$[HPW$_{12}$O$_{39}$] and [Cu(4,4'-bipy)$_4$][HPW$_{12}$O$_{40}$].

The SEM/EDX results of the (4,4'-bipy)$_3$[HPW$_{12}$O$_{39}$] crystal are shown in Table 4.1. In accordance with the results, the synthesized compound contains tungsten, carbon, oxygen, nitrogen and phosphorus elements in the weight percentages of 36.06%, 25.17%, 24.90%, 7.31% and 1.87% respectively.

Table 4.1. SEM/EDX results of (4,4'-bipy)$_3$[HPW$_{12}$O$_{39}$].

Element	Wt%
C	25.17
N	7.31
O	24.90
P	1.87
W	36.06

In conformity with the SEM/EDX results of [Cu(4,4'-bipy)$_4$][HPW$_{12}$O$_{40}$] (Table 4.2), the synthesized compound contains oxygen, carbon, tungsten,copper and nitrogen in the weight percentages of 31.66%, 26.43%, 24.38%, 7.48% and 7.38% respectively.

Table 4.2. SEM/EDX results of $[Cu(4,4'\text{-bipy})_4][HPW_{12}O_{40}]$.

Element	Wt%
C	26.43
N	7.38
O	31.66
P	1.72
Cu	7.48
W	24.38

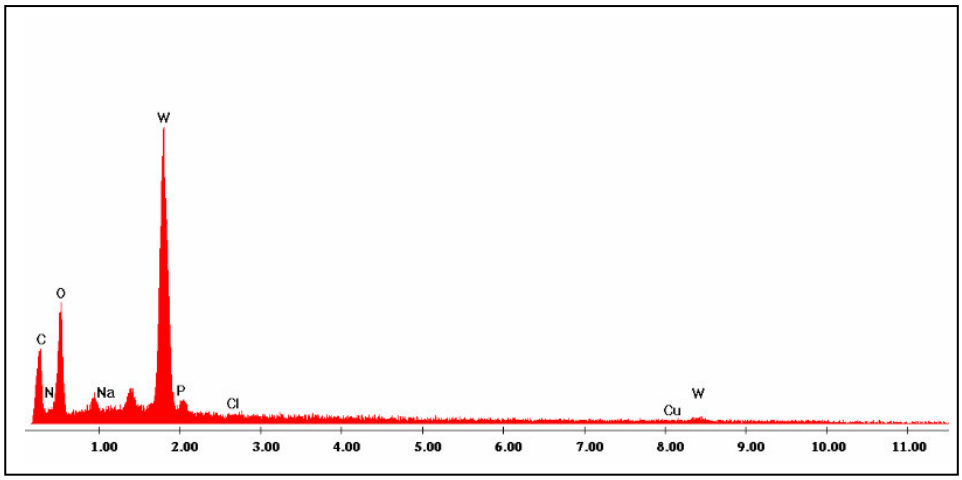

Figure 4.5. SEM/EDX spectrum of $(4,4'\text{-bipy})_3[HPW_{12}O_{39}]$.

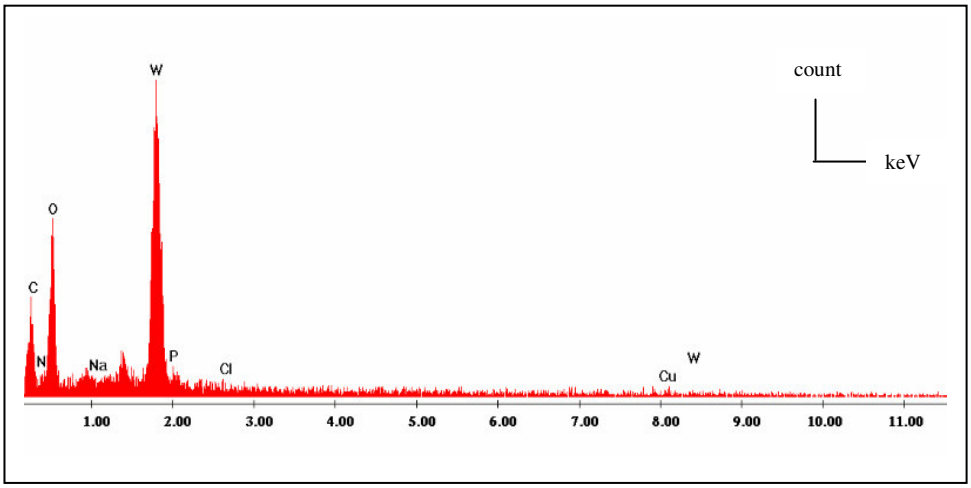

Figure 4.6. SEM/EDX spectrum of $[Cu(4,4'\text{-bipy})_4][HPW_{12}O_{40}]$.

The infrared spectra of both $(4,4'\text{-bipy})_3[HPW_{12}O_{39}]$ and $[Cu(4,4'\text{-bipy})_4][HPW_{12}O_{40}]$, which are shown in Figure 4.7 and Figure 4.8 respectively, were measured on a Perkin Elmer Spectrum 100 FT-IR spectrometer using KBr pellets in 4000 - 450 cm^{-1} region.

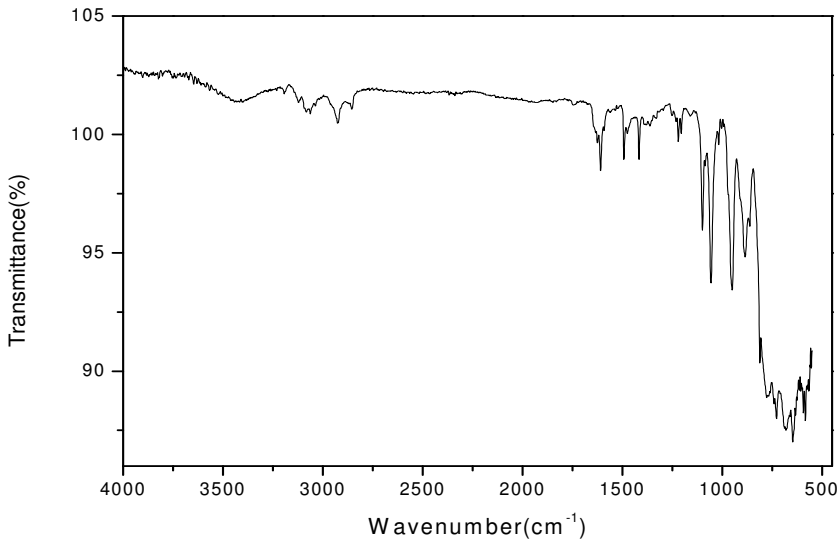

Figure 4.7. FT-IR spectrum of $(4,4'\text{-bipy})_3[HPW_{12}O_{39}]$.

The IR spectrum of (4,4'-bipy)$_3$[HPW$_{12}$O$_{39}$] (Figure 4.7) exhibits characteristic bands of 4,4'-bipyridine in 1200-3100 cm^{-1} range. Peaks in 3000-3100 cm^{-1} are assigned to υ(C-H), peaks in 1200-1700 cm^{-1} region are due to υ(C=C) and υ(C=N), and peaks at 1101 and 1059 cm^{-1} are assigned to υ_{as}(P-O) vibrations. The peaks between 900 and 956 cm^{-1} are due to υ(W=O) and the bands between 550-800 cm^{-1} are attributed to υ(W-O-W) modes.

The IR spectrum of [Cu(4,4'-bipy)$_4$][HPW$_{12}$O$_{40}$] (Figure 4.8) is similar to the spectrum of (4,4'-bipy)$_3$[HPW$_{12}$O$_{39}$]. The absorptions between 1200 and 1650 cm^{-1} are assigned to the characteristic peaks of 4,4'-bipyridine coordinated to Cu^{2+} ion. Peaks around 3000 cm^{-1} are assigned to υ(C-H). The peak at 1081 cm^{-1} is attributed to asymmetric P-O vibration. The peaks between 500 and 900 cm^{-1} are assigned to W=O and O-W-O vibrations.

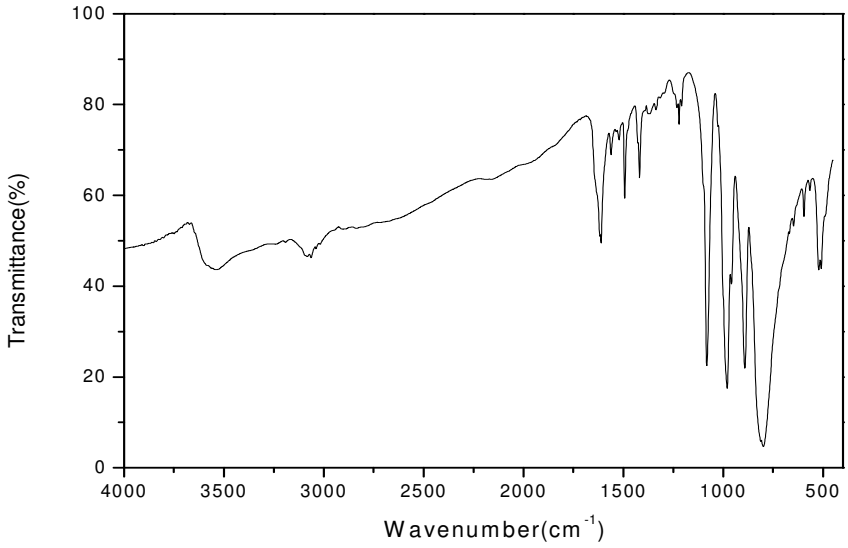

Figure 4.8. FT-IR spectrum of [Cu(4,4'-bipy)$_4$][HPW$_{12}$O$_{40}$].

4.2.1.2. X-ray Crystallographic Analysis of (4,4'-bipy)$_3$[HPW$_{12}$O$_{39}$] and [Cu(4,4'-bipy)$_4$][HPW$_{12}$O$_{40}$]

4.2.1.2.1. X-ray Crystallographic Analysis of (4,4'-bipy)$_3$[HPW$_{12}$O$_{39}$]

Single crystal X-ray diffraction analysis was done for green rod-like crystals of (4,4'-bipy)$_3$[HPW$_{12}$O$_{39}$]. The structure of the compound was solved by direct methods using the program SHELXS-97 (Sheldrick, 1990) and by refined full-matrix least-squares techniques using the program SHELXL-97 (Sheldrick, 1997).

Crystallographic data are given in Table 4.3. Bond lengths (Å) and bond angles (degree) for (4,4'-bipy)$_3$[HPW$_{12}$O$_{39}$] are given in Table 4.4 and Table 4.5. Final values of the atomic coordinates and isotropic displacement parameters are given in Table 4.6.

Table 4.3. Crystallographic data for (4,4'-bipy)$_3$[HPW$_{12}$O$_{39}$].

Formula	(4,4'-bipy)$_3$[HPW$_{12}$O$_{39}$]
Formula weight	3335.77
Crystal system	Monoclinic
Space group	P2$_1$/*n*
Cell formula units, Z	4
Description	Green rod-like block crystals
Unit cell dimensions	a=13.503(3) Å b=26.726(5) Å c=15.169(3) Å
Volume (Å^3)	5397.3(19)

Table 4.4. Selected bond lengths (Å) for (4,4'-bipy)$_3$[HPW$_{12}$O$_{39}$].

W(1)-O(39)	1.73(3)	W(10)-O(19)	2.40(3)	C(18)-C(20)	1.40(6)
W(1)-O(11)	1.96(2)	W(11)-O(29)	1.90(2)	C(22)-C(23)	1.34(5)
W(1)-O(18)	2.45(2)	W(11)-O(19)	2.43(2)	N(1)-C(11)	1.28(5)
W(2)-O(37)	1.71(3)	W(12)-O(16)	1.99(2)	N(2)-C(19)	1.43(5)
W(2)-O(21)	1.91(2)	W(12)-O(20)	2.43(2)	N(3)-C(14)	1.29(5)
W(2)-O(20)	2.41(2)	P(1)-O(18)	1.54(3)	N(4)-C(18)	1.32(5)
W(3)-O(38)	1.69(2)	P(1)-O(17)	1.55(2)	N(4)-C(21)	1.35(5)
W(3)- O(8)	1.83(2)	P(1)-O(20)	1.56(2)	N(5)-C(22)	1.39(5)
W(3)-O(25)	1.98(2)	C(1)-C(10)	1.34(5)	N(5)-C(25)	1.42(6)
W(4)-O(36)	1.69(2)	C(2)-C(4)	1.38(5)	N(6)-C(29)	1.36(5)
W(4)-O(17)	2.42(2)	C(3)-C(9)	1.30(5)		
W(5)-O(25)	1.92(2)	C(3)-C(4)	1.48(4)		
W(5)-O(18)	2.44(2)	C(3)-C(7)	1.51(4)		
W(6)-O(32)	1.74(2)	C(5)-C(8)	1.35(5)		
W(6)-O(17)	2.45(2)	C(5)-C(10)	1.40(5)		
W(7)-O(26)	1.70(2)	C(5)-C(12)	1.50(5)		
W(7)-O(19)	2.37(2)	C(6)-C(13)	1.41(5)		
W(8)-O(20)	2.37(2)	C(7)-C(24)	1.43(5)		
W(8)-O(14)	1.95(2)	C(8)-C(11)	1.41(5)		
W(8)-O(5)	1.85(2)	C(9)-C(19)	1.40(6)		
W(9)-O(31)	1.98(2)	C(12)-C(17)	1.44(4)		
W(9)-O(17)	2.46(2)	C(13)-C(14)	1.40(5)		
W(10)-O(35)	1.65(3)	C(17)-C(21)	1.30(6)		

Table 4.5. Selected bond angles (°) for (4,4'-bipy)$_3$[HPW$_{12}$O$_{39}$].

O(39)-W(1)- O(22)	104.3(11)	O(38)- W(3)-O(18)	168.5(11)	O(6)- W(4) –O(17)	83.7(8)
O(39)-W(1)- O(14)	103.7(10)	O(8)-W(3) –O(18)	85.0(9)	O(23) –W(4)–O(17)	71.4(8)
O(22) –W(1)-O(14)	86.4(10)	O(10)- W(3)- O(18)	83.6(9)	O(34)-W(5)- O(28)	103.0(10)
O(39)- W(1)–O(15)	102.4(11)	O(15)–W(3)–O(18)	71.4(8)	O(34)- W(5)- O(11)	100.1(10)
O(22)- W(1)- O(15)	89.0(10)	O(25) –W(3)- O(18)	72.3(9)	O(28) –W(5)- O(11)	156.8(9)
O(14) –W(1)-O(15)	153.9(9)	O(36) –W(4)- O(13)	102.6(10)	O(34)- W(5) –O(25)	99.7(10)
O(39)- W(1)- O(11)	99.5(11)	O(36)- W(4) –O(9)	99.1(12)	O(28)- W(5) –O(25)	90.2(10)
O(22) –W(1)-O(11)	156.1(10)	O(13) –W(4)- O(9)	89.3(9)	O(11)- W(5) –O(25)	87.8(9)
O(14)- W(1)- O(11)	86.9(9)	O(36) –W(4) –O(6)	104.1(12)	O(34)- W(5)- O(1)	102.2(10)
O(15) –W(1)-O(11)	87.1(9)	O(13) –W(4) –O(6)	89.0(9)	O(28) –W(5) –O(1)	86.3(10)
O(39) –W(1)-O(18)	169.6(10)	O(9) –W(4)- O(6)	156.5(10)	O(11) –W(5)- O(1)	87.0(9)
O(22) –W(1)-O(18)	84.6(10)	O(36) –W(4) –O(23)	100.7(10)	O(25) –W(5) –O(1)	158.1(10)
O(14) –W(1)-O(18)	82.1(8)	O(13) –W(4)- O(23)	156.7(10)	O(34) –W(5)- O(18)	170.5(9)
O(15) –W(1)-O(18)	71.9(9)	O(9) –W(4) –O(23)	86.0(10)	O(28) –W(5)-O(18)	83.9(9)
O(11) –W(1)-O(18)	71.8(9)	O(38)- W(3)- O(15)	100.2(11)	O(11) –W(5)- O(18)	73.4(8)
O(37) –W(2)-O(16)	98.4(11)	O(8) –W(3) –O(15)	156.4(9)	O(25) –W(5)-O(18)	73.5(9)
O(37)–W(2)- O(21)	104.6(10)	O(10)- W(3)- O(15)	86.9(10)	O(1) –W(5)- O(18)	84.5(9)
O(16) –W(2)-O(21)	91.6(10)	O(38) –W(3) –O(25)	99.6(11)	O(32) –W(6)-O(31)	103.0(12)
O(37) –W(2)-O(24)	99.6(11)	O(8) –W(3)- O(25)	89.1(10)	O(32) –W(6)- O(22)	104.3(12)
O(16)- W(2)- O(24)	88.9(10)	O(10) –W(3)- O(25)	155.9(9)	O(31) –W(6)-O(22)	89.9(10)
O(21) –W(2)-O(24)	155.4(10)	O(15) –W(3)- O(25)	84.7(9)	O(32)- W(6)- O(2)	101.5(12)
O(37)- W(2)- O(1)	101.8(11)	O(38) –W(3) –O(18)	168.5(11)	O(31) –W(6) –O(2)	155.5(10)

(cont. on next page)

Table 4.5. (cont.)

O(33)- W(7)-O(28)	157.8(10)	O(24)-W(8)-O(20)	72.1(8)	O(13)–W(12)-O(5)	89.8(9)
O(26)–W(7)-O(21)	100.6(10)	O(27)–W(9)-O(29)	101.8(12)	O(4) –W(12)-O(16)	102.0(9)
O(7)–W(7)–O(21)	157.1(10)	O(27) –W(9)-O(23)	102.8(10)	O(3) –W(12)- O(16)	89.9(10)
O(33)-W(7)-O(21)	85.1(10)	O(29) –W(9)-O(23)	90.0(10)	O(13)–W(12)-O(16)	159.6(9)
O(28)-W(7)-O(21)	82.6(10)	O(27) –W(9)-O(10)	102.7(11)	O(5)–W(12)-O(16)	84.6(10)
O(26)- W(7)-O(19)	171.2(10)	O(29) –W(9)-O(10)	87.9(10)	O(4) –W(12)–O(20)	171.3(9)
O(7) –W(7)-O(19)	76.0(9)	O(23) –W(9)-O(10)	154.3(9)	O(3)–W(12)-O(20)	87.5(9)
O(33)- W(7)-O(19)	73.8(10)	O(27) –W(9)-O(31)	101.2(11)	O(13)–W(12)-O(20)	86.0(9)
O(28)–W(7)-O(19)	86.1(9)	O(29) –W(9)-O(31)	156.9(11)	O(5)–W(12)-O(20)	72.1(9)
O(21)–W(7)-O(19)	81.5(8)	O(23) –W(9)-O(31)	85.7(10)	O(16)–W(12)-O(20)	73.6(8)
O(30) –W(8)–O(5)	101.2(11)	O(10)-W(9)-O(31)	86.2(10)	O(18)- P(1)-O(19)	109.2(13)
O(30) –W(8)-O(2)	103.8(11)	O(27) –W(9)–O(17)	170.0(9)	O(18) –P(1) –O(17)	109.2(12)
O(5) –W(8) –O(2)	93.3(10)	O(29) –W(9)-O(17)	86.5(9)	O(19) –P(1) –O(17)	111.1(12)
O(30)–W(8)-O(14)	103.4(10)	O(23)–W(9)–O(17)	71.3(8)	O(18) –P(1) -O(20)	107.8(13)
O(5)–W(8)–O(14)	155.4(9)	O(10)-W(9)- O(17)	82.9(8)	O(19) –P(1) -O(20)	110.7(13)
O(2)–W(8)- O(14)	83.1(9)	O(31)–W(9)–O(17)	70.6(8)	O(17) –P(1) –O(20)	108.8(13)
O(30)- W(8)- O(24)	99.3(11)	O(35)–W(10)- O(3)	101.0(12)	C(11)- N(1)- C(1)	123(3)
O(5) –W(8)- O(24)	90.6(10)	O(35)–W(10)-O(12)	100.1(11)	C(2)- N(2)- C(199	119(4)

(cont. on next page)

Table 4.5. (cont.)

O(5)–W(8)-O(20)	75.3(9)	O(12) –W(10)- O(6)	87.6(9)	C(28)- C(27)-C(6)	126(3)
O(2)–W(8)-O(20)	85.3(9)	O(35) –W(10)–O(33)	100.8(11)	C(30)–C(28)-C(27)	121(4)
O(14)-W(8)-O(20)	80.1(8)	O(3) –W(10)- O(33)	86.7(10)	C(26)- C(29)-N(6)	120(3)
O(30) –W(8)-O(20)	170.5(10)	N(2) –C(2) –C(4)	125(3)	C(28)–C(30)–N(6)	120(4)
O(14) –W(8)-O(24)	83.3(10)	O(35) –W(10)- O(6)	102.7(12)	C(18)-N(4)-C(21)	119(4)
O(3) –W(10)- O(6)	88.8(9)	C(9) –C(3) –C(4)	122(3)	C(22)–N(5)–C(25)	117(4)
O(4) –W(12)-O(5)	100.2(11)	C(9)- C(3)- C(7)	121(3)		
C(12)- C(20)-C(18)	121(4)	N(1) –C(1) –C(10)	122(3)		
C(16) –C(6)–C(13)	116(3)	C(17)- C(12)- C(5)	118(4)		
C(16) –C(6)-C(27)	125(3)	C(14) –C(13) –C(6)	119(3)		
C(13)- C(6)–C(27)	119(3)	N(3) –C(14)- C(13)	122(4)		
C(23) –C(7)–C(24)	113(3)	C(16) –C(15)- N(3)	121(4)		
C(23) –C(7)–C(3)	123(3)	C(15) –C(16)- C(6)	123(4)		
C(24) –C(7)–C(3)	124(3)	C(21) –C(17) –C(12)	116(4)		
C(5) –C(8)-C(11)	121(4)	C(4)- C(3)- C(7)	117(3)		
C(3) –C(9)–C(19)	120(4)	C(4) –C(3) –C(7)	117(3)		
C(1) –C(10) –C(5)	117(4)	C(8) –C(5) –C(10)	118(3)		
N(1) –C(11)–C(8)	118(4)	C(29) –C(26)- C(27)	121(3)		
C(20)–C(12)-C(17)	118(4)	C(26) –C(27)- C(28)	117(3)		
C(20) –C(12)- C(5)	124(3)	C(26)- C(27)- C(6)	117(3)		

Table 4.6. İsotropic coordinates for (4,4'-bipy)$_3$[HPW$_{12}$O$_{39}$].

Atom	x	y	z	Ueq
W1	0.17705(10)	0.01663(5)	0.73768(9)	0.0138(3)
W2	-0.07437(9)	0.15705(5)	0.71005(8)	0.0122(3)
W3	0.34815(10)	0.08498(5)	0.88411(8)	0.0146(3)
W4	0.28779(10)	0.19720(5)	0.52505(8)	0.0139(3)
W5	0.09530(10)	0.09223(5)	0.89315(8)	0.0128(3)
W6	0.28045(10)	0.06932(5)	0.54906(9)	0.0143(3)
W7	0.11467(10)	0.22999(5)	0.87021(8)	0.0122(3)
W8	0.00639(10)	0.08203(5)	0.55420(8)	0.0139(3)
W9	0.44871(10)	0.13915(5)	0.69501(9)	0.0159(3)
W10	0.20165(10)	0.28009(5)	0.69148(9)	0.0150(3)
W11	0.35910(16)	0.22060(8)	0.85628(13)	0.0428(5)
W12	0.02234(15)	0.20664(8)	0.53592(13)	0.0397(5)
P1	0.1873(6)	0.1486(3)	0.7089(5)	0.0122(17)
O1	-0.0150(18)	0.1098(8)	0.8015(14)	0.015(5)
O2	0.1369(16)	0.0752(8)	0.5224(14)	0.013(5)
O3	0.0839(18)	0.2575(9)	0.6172(15)	0.018(5)
O4	-0.0394(18)	0.2476(9)	0.4387(17)	0.023(6)
O5	-0.0207(18)	0.1405(8)	0.4899(15)	0.016(5)
O6	0.2785(15)	0.2491(9)	0.6127(14)	0.014(5)
O7	0.2476(16)	0.2371(9)	0.9204(15)	0.015(5)
O8	0.3546(16)	0.1521(8)	0.9067(15)	0.014(5)
O9	0.2901(16)	0.1313(8)	0.4811(14)	0.012(5)
O10	0.4143(17)	0.0952(9)	0.7842(14)	0.016(5)
O11	0.0996(16)	0.0305(9)	0.8333(14)	0.016(5)

(cont. on next page)

Table 4.6. (cont.)

Atom	x	y	z	Ueq
O12	0.3182(19)	0.2781(9)	0.7800(15)	0.018(5)
O13	0.1506(15)	0.1966(8)	0.4976(16)	0.014(5)
O14	0.0650(15)	0.0415(8)	0.6568(16)	0.016(5)
O15	0.2946(16)	0.0236(8)	0.8256(15)	0.014(5)
O16	-0.0876(15)	0.1996(9)	0.6079(14)	0.015(5)
O17	0.2658(15)	0.1414(8)	0.6462(13)	0.014(5)
O18	0.1973(16)	0.1055(9)	0.7771(16)	0.012(5)
O19	0.2031(15)	0.1987(9)	0.7591(14)	0.016(5)
O20	0.0799(17)	0.1459(9)	0.6520(17)	0.016(5)
O21	-0.0008(17)	0.2069(9)	0.7836(14)	0.018(5)
O22	0.2539(19)	0.0323(9)	0.6495(15)	0.014(5)
O23	0.4195(15)	0.1821(10)	0.5942(15)	0.015(5)
O24	-0.0903(19)	0.1006(9)	0.6319(15)	0.014(5)
O25	0.2318(18)	0.0806(8)	0.9477(15)	0.012(5)
O26	0.0549(17)	0.2613(8)	0.9439(14)	0.009(4)
O27	0.5757(16)	0.1345(10)	0.7101(14)	0.017(5)
O28	0.1131(18)	0.1610(10)	0.9121(14)	0.015(5)
O29	0.4308(19)	0.1924(9)	0.7703(15)	0.019(5)
O30	-0.0646(19)	0.0405(10)	0.4869(16)	0.014(5)
O31	0.4084(17)	0.0840(9)	0.6095(15)	0.023(6)
O32	0.303(2)	0.0238(10)	0.4727(17)	0.016(5)
O33	0.1206(18)	0.2835(9)	0.7884(16)	0.014(5)

(cont. on next page)

Table 4.6. (cont.)

Atom	x	y	z	Ueq
O34	0.0352(17)	0.0741(8)	0.9792(14)	0.013(5)
O35	0.203(2)	0.3395(9)	0.6621(16)	0.024(6)
O36	0.3212(16)	0.2283(11)	0.4372(16)	0.023(6)
O37	-0.194(2)	0.1620(9)	0.7315(17)	0.025(6)
O38	0.4383(18)	0.0612(10)	0.9635(15)	0.022(6)
O39	0.1624(18)	-0.0476(9)	0.7304(16)	0.021(5)
N1	0.534(2)	0.2937(11)	0.707(2)	0.022(7)
H1B	0.5656	0.2729	0.7452	0.027
N2	-0.094(2)	0.0030(12)	0.7469(18)	0.022(7)
H2B	-0.0597	0.0291	0.7377	0.027
N3	0.579(2)	0.0036(11)	0.795(2)	0.024(7)
H3A	0.6173	0.0226	0.8320	0.029
N4	0.192(2)	0.4340(11)	0.417(2)	0.028(8)
H4C	0.1478	0.4495	0.3797	0.033
N5	-0.412(2) -	-0.2007(14)	0.8069(17)	0.027(8)
H5A	-0.4588	0.222	0.8118	0.032
N6	0.259(3)	-0.1511(12)	0.5037(17)	0.024(7)
H6A	0.216	-0.1684	0.4679	0.029
C1	0.495(3)	0.3336(13)	0.738(2)	0.020(8)
H1A	0.5119	0.3413	0.7983	0.025

(cont. on next page)

Table 4.6. (cont.)

Atom	x	y	z	Ueq
C2	-0.116(2)	-0.0303(16)	0.686(2)	0.025(9)
H2A	-0.0923	0.0253	0.6323	0.03
C6	0.456(2)	-0.0600(13)	0.680(2)	0.016(7)
C7	-0.273(2)	-0.1231(14)	0.791(2)	0.015(7)
C8	0.463(3)	0.3150(15)	0.564(2)	0.032(10)
H8A	0.458	0.397	0.5023	0.039
C9	-0.179(2)	-0.0477(16)	0.846(3)	0.029(9)
H9A	-0.1958	0.0537	0.9022	0.035
C10	0.431(2)	0.3637(16)	0.685(2)	0.021(8)
H10	0.4017	0.3913	0.7082	0.025
C11	0.527(3)	0.2841(14)	0.624(3)	0.030(10)
H11	0.5619	0.2578	0.6039	0.036
C12	0.337(3)	0.3830(15)	0.531(2)	0.023(9)
C13	0.522(3)	-0.0259(15)	0.648(2)	0.026(9)
H13	0.5282	-0.025	0.5883	0.031
C14	0.579(3)	0.0066(14)	0.710(2)	0.024(8)
H14	0.6174	0.312	0.6887	0.029
C15	0.515(3)	-0.0319(15)	0.826(3)	0.030(9)
H15	0.5147	-0.0350	0.8869	0.037
C16	0.457(3) -	-0.0603(13)	0.770(2)	0.020(8)

(cont. on next page)

Table 4.6. (cont.)

Atom	x	y	z	Ueq
C17	0.287(4)	0.3601(17)	0.450(3)	0.057(17)
H17	0.303	0.3279	0.4332	0.069
C18	0.236(4) 0	0.4560(17)	0.491(2)	0.037(11)
H18	0.2201	0.4888	0.5031	0.044
C19	-0.127(3)	-0.0040(18)	0.831(3)	0.036
H19	-0.115	0.0204	0.875	0.036
C20	0.307(4)	0.4295(18)	0.551(2)	0.044(10)
H20	0.3347	0.4442	0.6047	0.042(13)
C21	0.219(4)	0.387(2)	0.401(3)	0.051
H21	0.1845	0.3717	0.3489	0.07(2)
C22	-0.400(3)	-0.1810(15)	0.724(3)	0.079
H22	-0.4387	-0.1939	0.6727	0.023(8)
C23	-0.336(3)	-0.1440(15)	0.717(3)	0.027
H23	-0.3323	-0.1315	0.665	0.028(9)
C24	-0.284(3)	-0.1457(18)	0.874(2)	0.034
H24	-0.2461	-0.1326	0.9253	0.035(11)
C25	-0.344(4)	-0.184(2)	0.883(3)	0.042
H25	-0.3410	-0.1999	0.9376	0.050(14)
C26	0.302(3)	-0.1098(13)	0.640(2)	0.06
H26	0.2871	-0.1012	0.6955	0.017(7)
C27	0.389(2)	-0.0912(13)	0.614(2)	0.02
C28	0.408(4)	-0.1061(14)	0.529(3)	0.014(7)
H28	0.4655	-0.0951	0.5093	0.043

(cont. on next page)

Table 4.6. (cont.)

Atom	x	y	z	Ueq
C29	0.240(2)	-0.1398(15)	0.587(3)	0.026(9)
H29	0.1841	-0.1530	0.6061	0.031
C30	0.344(3)	-0.1357(16)	0.477(2)	0.032(10)
H30	0.3577	-0.1458	0.4218	0.039

4.2.1.2.2. Results and Discussion for (4,4'-bipy)$_3$[HPW$_{12}$O$_{39}$]

The novel compound (4,4'-bipy)$_3$[HPW$_{12}$O$_{39}$] was obtained as green, rod-like crystals under hydrothermal conditions from the reaction of $Na_6[H_2W_{12}O_{40}]$, $CuCl_2.2H_2O$, 4,4'-bipyridine and H_3PO_4 at pH 2.3. The polyoxometalate (POM) unit of the structure is shown in Figure 4.9.

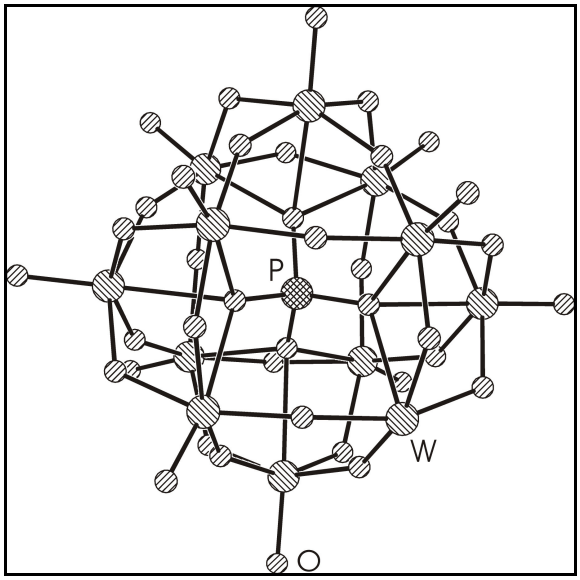

Figure 4.9. View of $[PW_{12}O_{39}]^{1-}$ cluster.

The title compound (4,4'-bipy)$_3$[HPW$_{12}$O$_{39}$] consists of [PW$_{12}$O$_{39}$]$^{1-}$ polyoxoanion clusters and 4,4'-bipyridine ligands. The basic building block of the structure, [PW$_{12}$O$_{39}$] $^{1-}$ polyanion, is a Keggin structure and consists of 12 edge- and corner-sharing WO$_6$ octahedra and a PO$_4$ tetrahedron at the center of the cluster. (Figure 4.9). The W-O bond distances in WO$_6$ octahedra can be divided into three groups: W-O$_t$ (terminal), whose bond distances range from 1.69(3) to 1.73(2) Å which indicate a W = O multiple bond. W-O$_b$ (bridging), varying from 1.90(2) to 1.97(2) Å and W-O$_c$ (central) from 2.37(2) to 2.46(2) Å. The P-O bond distances fall in the ranges of 1.54 - 1.56 Å. All of the bond distances are in accordance with the bonds of typical Keggin polyanions already existing in the literature.

The polyanion [PW$_{12}$O$_{39}$]$^{1-}$ shares its one oxygen with another [PW$_{12}$O$_{39}$]$^{1-}$ cluster. The regularity of this bonding forms 1D infinite chains as demonstrated in Figure 4.10. This type of condensed structures of POM clusters is intriguing. There are limited number of examples for condensed polyoxometalates in the literature. [Hen][Cu(en)$_2$(H$_2$O)]$_2$[Cu(en)$_2$(H$_2$O)$_2$]$_{0.5}$[{Cu(en)$_2$(H$_2$O)}$_2${Cu(en)$_2$}(P$_2$W$_{18}$O$_{61}$)$_2$]en. nH$_2$O and [HenMe]$_2$[Cu(enMe)$_2$][{Cu(enMe)$_2$}P$_2$W$_{18}$O$_{61}$].9H$_2$O are the first condensed structures formed by unsubstituted POM clusters through sharing common atoms. (Lin et.al., 2009)

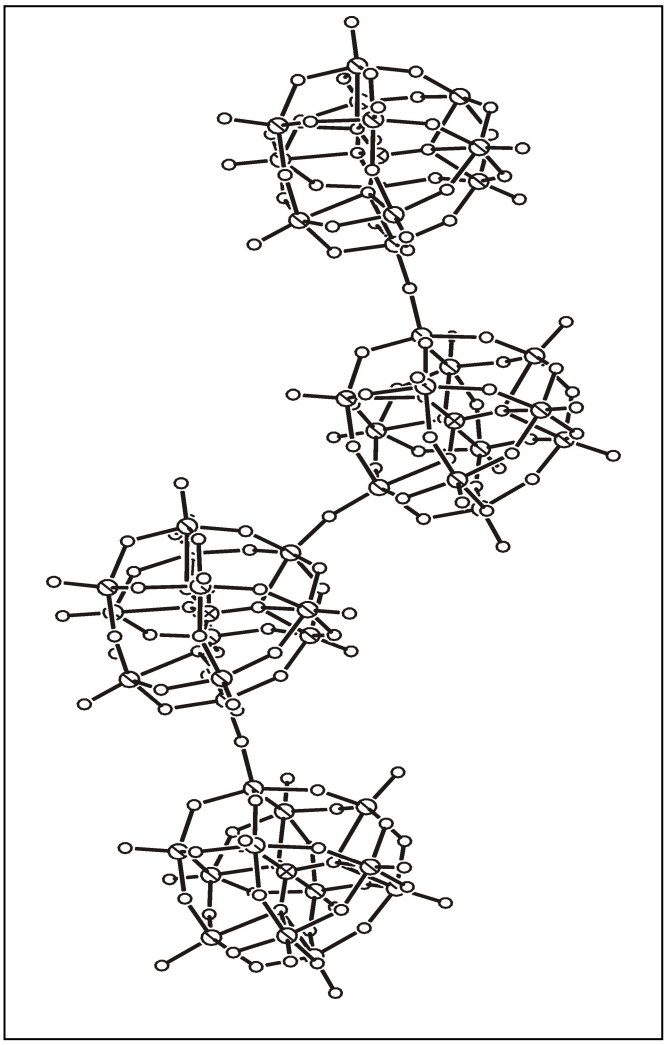

Figure 4.10. View of a chain composed of $[PW_{12}O_{39}]^{1-}$ polyanions.

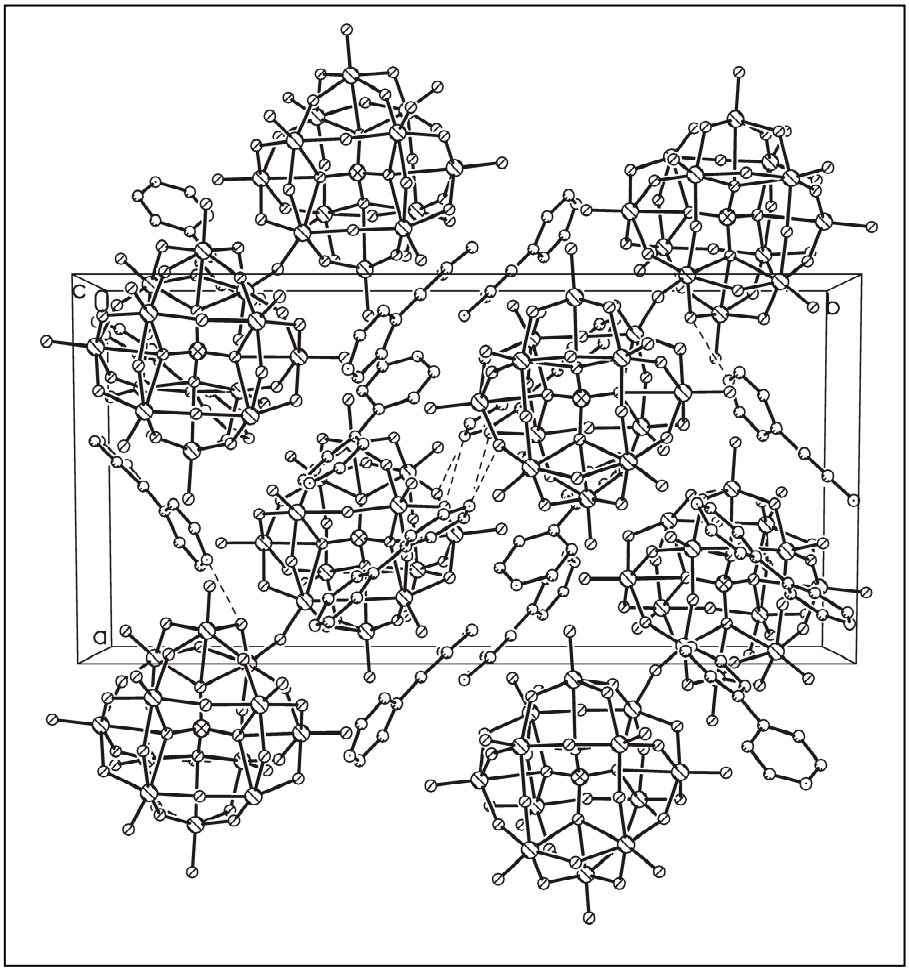

Figure 4.11. Unit cell view of (4,4'-bipy)$_3$[HPW$_{12}$O$_{39}$].

The unit cell of the title compound (Figure 4.11) includes $[PW_{12}O_{39}]^{1-}$ clusters, which are linked via oxygen atoms and 4,4'-bipyridine groups among these clusters. The discerete chains and 4,4'-bipyridine ligands coexist in the crystal lattice through C-H…O hydrogen bonding interactions.

4.2.1.2.3. X-ray Crystallographic Analysis of $[Cu(4,4'bipy)_4][HPW_{12}O_{40}]$

Single crystal X-ray diffraction analysis was done for purple, plate-like crystals $[Cu(4,4'\text{-bipy})_4][HPW_{12}O_{40}]$. The structure of the compound was solved by direct methods using the program SHELXS-97 (Sheldrick, 1990) and by refined full-matrix least-squares techniques using the program SHELXL-97 (Sheldrick, 1997).

Crystallographic data are given in Table 4.7. Bond lengths (Å) and bond angles (degree) for $[Cu(4,4'\text{-bipy})_4][HPW_{12}O_{40}]$ are given in Table 4.8 and Table 4.9 respectively. Final values of the atomic coordinates and isotropic displacement parameters are given in Table 4.10.

Table 4.7. Crystallographic data for $[Cu(4,4'\text{-bipy})_4][HPW_{12}O_{40}]$.

Formula	$[Cu(4,4'\text{-bipy})_4][HPW_{12}O_{40}]$
Formula weight	3321.39
Crystal system	Tetragonal
Space group	P*bcn*
Cell formula units, Z	8
Description	purple plate-like crystals
Unit cell dimensions	a=20.236(4) Å b=25.635(5) Å c=20.236 (4) Å
Volume ($Å^3$)	10497(4)

Table 4.8. Selected bond lengths (Å) for $[Cu(4,4'\text{-bipy})_4][HPW_{12}O_{40}]$.

W(1)-O(39)	1.73(3)	W(10)-O(19)	2.40(3)	C(18)-C(20)	1.40(6)
W(1)-O(11)	1.96(2)	W(11)-O(29)	1.90(2)	C(22)-C(23)	1.34(5)
W(1)-O(18)	2.45(2)	W(11)-O(19)	2.43(2)	N(1)-C(11)	1.28(5)
W(2)-O(37)	1.71(3)	W(12)-O(16)	1.99(2)	N(2)-C(19)	1.43(5)
W(2)-O(21)	1.91(2)	W(12)-O(20)	2.43(2)	N(3)-C(14)	1.29(5)
W(2)-O(20)	2.41(2)	P(1)-O(18)	1.54(3)	N(4)-C(18)	1.32(5)
W(3)-O(38)	1.69(2)	P(1)-O(17)	1.55(2)	N(4)-C(21)	1.35(5)
W(3)- O(8)	1.83(2)	P(1)-O(20)	1.56(2)	N(5)-C(22)	1.39(5)
W(3)-O(25)	1.98(2)	C(1)-C(10)	1.34(5)	N(5)-C(25)	1.42(6)
W(4)-O(36)	1.69(2)	C(2)-C(4)	1.38(5)	N(6)-C(29)	1.36(5)
W(4)-O(17)	2.42(2)	C(3)-C(9)	1.30(5)		
W(5)-O(25)	1.92(2)	C(3)-C(4)	1.48(4)		
W(5)-O(18)	2.44(2)	C(3)-C(7)	1.51(4)		
W(6)-O(32)	1.74(2)	C(5)-C(8)	1.35(5)		
W(6)-O(17)	2.45(2)	C(5)-C(10)	1.40(5)		
W(7)-O(26)	1.70(2)	C(5)-C(12)	1.50(5)		
W(7)-O(19)	2.37(2)	C(6)-C(13)	1.41(5)		
W(8)-O(20)	2.37(2)	C(7)-C(24)	1.43(5)		
W(8)-O(14)	1.95(2)	C(8)-C(11)	1.41(5)		
W(8)-O(5)	1.85(2)	C(9)-C(19)	1.40(6)		
W(9)-O(31)	1.98(2)	C(12)-C(17)	1.44(4)		
W(9)-O(17)	2.46(2)	C(13)-C(14)	1.40(5)		

Table 4.9. Selected bond angles (°) for $[Cu(4,4'\text{-bipy})_4][HPW_{12}O_{40}]$.

O(31)-W(1)O(6)	102.5(12)	O(24)-W(2)-O(3)	84.6(9)	O(37)-W(4)-O(20)	102.3(12)
O(31)-W(1)-O(14)	100.2(11)	O(4)-W(2)-O(32)	171.0(10)	O(1)-W(4)-O(20)	153.7(11)
O(6)-W(1)-O(14)	91.0(9)	O(11)-W(2)-O(32)	83.2(9)	O(34)-W(4)-O(20)	89.7(12)
O(31)-W(1)-O(2)	101.9(10)	O(30)-W(2)-O(32)	83.6(10)	O(37)-W(4)-O(16)	101.1(11)
O(6)-W(1)-O(2)	155.5(9)	O(24)-W(2)-O(32)	71.5(9)	O(1)-W(4)-O(16)	87.1(9)
O(14)-W(1)-O(2)	86.6(9)	O(3)-W(2)-O(32)	72.1(9)	O(34)-W(4)-O(16)	155.5(10)
O(31)-W(1)-O(30)	103.6(11)	O(7)-W(3)-O(8)	106.2(10)	O(20)-W(4)-O(16)	88.3(11)
O(6)-W(1)-O(30)	83.3(10)	O(7)-W(3)-O(12)	102.8(11)	O(37)-W(4)-O(40)	171.5(11)
O(14)-W(1)-O(30)	156.2(9)	O(8)-W(3)-O(12)	84.6(9)	O(1)-W(4)-O(40)	79.6(9)
O(2)-W(1)-O(30)	89.1(9)	O(7)-W(3)-O(18)	100.0(9)	O(34)-W(4)-O(40)	84.8(10)
O(31)-W(1)-O(19)	171.3(11)	O(8)-W(3)-O(18)	153.8(8)	O(20)-W(4)-O(40)	74.4(10)
O(6)-W(1)-O(19)	83.0(9)	O(12)-W(3)-O(18)	89.2(10)	O(16)-W(4)-O(40)	71.2(9)
O(14)-W(1)-O(19)	72.9(9)	O(7)-W(3)-O(2)	102.2(10)	O(10)-W(5)-O(26)	102.1(10)
O(2)-W(1)-O(19)	73.0(7)	O(8)-W(3)-O(2)	88.2(8)	O(10)-W(5)-O(12)	101.3(10)
O(30)-W(1)-O(19)	83.5(8)	O(12)-W(3)-O(2)	155.0(9)	O(26)-W(5)- O(12)	84.8(9)
O(4)-W(2)-O(11)	103.4(11)	O(18)-W(3)-O(2)	86.8(9)	O(10)- W(5)-O(5)	104.3(8)
O(4)-W(2)-O(30)	103.1(10)	O(7)-W(3)-O(19)	169.3(9)	O(26)- W(5)-O(5)	153.6(9)
O(11)-W(2)-O(30)	84.2(11)	O(8)-W(3)-O(19)	82.1(8)	O(12) –W(5)-O(5)	88.6(9)
O(4)-W(2)-O(24)	102.1(10)	O(12)-W(3)-O(19)	84.4(8)	O(10)-W(5)-O(36)	101.5(10)
O(11)-W(2)-O(24)	154.5(10)	O(18)-W(3)-O(19)	72.0(8)	O(26)-W(5)-O(36)	88.8(10)
O(30)-W(2)-O(24)	90.0(11)	O(2)-W(3)-O(19)	70.8(8)	O(12)-W(5)-O(36)	157.2(9)
O(4)-W(2)-O(3)	101.4(10)	O(37)-W(4)-O(1)	103.9(11)	O(5)-W(5)-O(36)	87.4(10)
O(11)-W(2)-O(3)	90.5(10)	O(37)-W(4)-O(34)	103.2(12)	O(10)- W(5)-O(22)	174.4(10)
O(30)-W(2)-O(3)	155.5(9)	O(1)-W(4)-O(349	83.9(10)	O(26)-W(5)-O(22)	81.1(9)

(cont. on next page)

Table 4.9. (cont.)

O(28)-W(6)-O9	103.1(11)	O(39)-W(8)-O(5)	100.1(12)	O(24)-W(9)-O(32)	72.7(8)
O(28)-W(6)-O(36)	102.6(11)	O(21)-W(8)-O(5)	154.8(10)	O(33)-W(9)-O(32)	71.0(10)
O(28)-W(6)-O(38)	102.4(12)	O(21)-W(8)-O(38)	89.1(11)	O(23)-W(10)-O(27)	102.3(11)
O(9)-W(6)-O(38)	154.4(11)	O(5)-W(8)-O(38)	86.9(10)	O(23)-W(10)-O(16)	104.6(10)
O(36)-W(6)-O(38)	85.8(11)	O(39)-W(8)-O(15)	100.4(12)	O(27)-W(10)-O(16)	89.5(11)
O(28)-W(6)-O(8)	100.6(12)	O(21)-W(8)-O(15)	85.8(9)	O(23)-W(10)-O(6)	102.2(11)
O(9)-W(6)-O(34)	83.5(11)	O(5)-W(8)-O(15)	88.1(9)	O(27)-W(10)-O(6)	88.5(11)
O(36)-W(6)- O(34)	156.9(10)	O(38)-W(8)-O(15)	156.6(11)	O(16)-W(10)-O(6)	153.0(9)
O(38)–W(6)-O(34)	89.7(11)	O(39)-W(8)-O(22)	170.8(12)	O(23)-W(10) O(11)	102.1(11)
O(28)–W(6)–O(22)	173.5(10)	O(21)-W(8)-O(22)	83.3(9)	O(27)-W(10)-O(11)	154.9(9)
O(9) –W(6)- O(22)	81.6(8)	O(5)-W(8)-O(22)	71.8(8)	O(16)-W(10)-O(11)	90.1(9)
O(36)-W(6)-O(22)	72.6(8)	O(38)-W(8)-O(22)	72.8(10)	O(6)-W(10)-O(11)	80.6(10)
O(38)–W(6)–O(22)	73.2(10)	O(15)–W(8)-O(22)	83.9(9)	O(23)-W(10)-O(40)	173.8(9)
O(34)–W(6)-O(22)	84.3(9)	O(29)-W(9)-O(8)	102.3(11)	O(27)-W(10)-O(40)	74.7(9)
O(13)–W(7)–O(25)	104.3(11)	O(29)-W(9)-O(24)	102.9(10)	O(16)-W(10)-O(40)	70.3(8)
O(13)-W(7)-O(20)	100.5(12)	O(8)-W(9)-O(24)	90.6(10)	O(6)-W(10)-O(40)	83.2(9)
O(25)-W(7)-O(20)	155.2(11)	O(29)-W(9)-O(33)	103.4(11)	O(11)-W(10)-O(40)	81.6(9)
O(13)-W(7)-O(21)	103.6(11)	O(8)-W(9)-O(33)	154.3(10)	O(35)-W(11)-O(33)	102.7(11)
O(25)-W(7)-O(21)	84.8(9)	O(24)-W(9)-O(33)	85.1(10)	O(35)-W(11)-O(9)	106.5(11)
O(20)-W(7)-O(21)	88.1(11)	O(29)-W(9)-O(26)	101.5(10)	O(33)-W(11)-O(9)	88.5(11)
O(13)-W(7)-O(27)	104.8(11)	O(8)-W(9)-O(26)	85.0(9)	O(35)-W(11)-O(3)	98.0(11)
O(25)-W(7)-O(27)	87.5(10)	O(24)-W(9)-O(26)	155.7(9)	O(33) –W(11)-O(3)	86.4(9)
C(22)-N(6)-C(22)	127(5)	N(2)-C(2)- C(1)	122(3)		
C(2)–C(1)-C(3)	116(3)	N(1)-C(16)-C(14)	115(3)		
C(5)-C(3)-C(1)	120(3)	C(15)-C(17)-C(18)	114(2)		

(cont. on next page)

Table 4.9. (cont.)

C(5)-C(3)-C(10)	122(3)	C(18)-C(17)-C(18)	132(4)
C(1)-C(3)-C(10)	118(3)	C(21)-C(18)-C(17)	106(4)
N(3)-C(4)-C(8)	126(3)	C(7)-C(19)-C(22)	116(3)
C(3)-C(5)-C(12)	116(3)	C(11)-C(20)-N(5)	108(5)
C(8)-C(6)-C(8)	127(4)	N(4)-C(21)-C(18)	120(4)
C(8)-C(6)-C(7)	117(2)	N(6)-C(22)-C(19)	120(4)
C(8)-C(6)-C(7)	117(2)		
C(19)-C(7)-C(19)	121(4)		
C(19)-C(7)-C(6)	119.3(19)		
C(6)-C(8)-C(4)	111(3)		
C(13)-C(9)-C(10)	116(4)		
C(9)-C(10)-C(11)	126(4)		
C(9)-C(10)-C(3)	121(4)		
C(11)-C(10)-C(3)	112(4)		
C(20)-C(11)-C(10)	117(5)		
N(2)-C(12)-C(5)	123(3)		
C(9)-C(13)-N(5)	118(4)		
C(15)-C(14)-C(16)	125(4)		
C(14)-C(15)-C(14)	115(6)		
C(14)-C(15)-C(17)	122(3)		

Table 4.10. İsotropic coordinates for $[Cu(4,4'\text{-bipy})_4][HPW_{12}O_{40}]$.

Atom	x	y	z	Ueq
W1	0.21543(7)	0.41958(5)	0.92057(7)	0.0292(3)
W2	0.17523(7)	0.41728(5)	1.09742(8)	0.0298(4)
W3	0.38006(7)	0.40878(5)	0.95623(7)	0.0282(3)
W4	0.15230(7)	0.22171(5)	1.08063(8)	0.0326(4)
W5	0.43841(7)	0.29950(5)	1.06011(8)	0.0301(4)
W6	0.32933(7)	0.21063(5)	1.12124(8)	0.0336(4)
W7	0.18890(7)	0.22464(5)	0.91558(8)	0.0325(4)
W8	0.36581(7)	0.21326(5)	0.95573(8)	0.0327(4)
W9	0.33917(7)	0.40552(5)	1.13358(7)	0.0278(3)
W10	0.09711(7)	0.32225(5	0.98541(8)	0.0319(4
W11	0.22916(7)	0.31610(5	1.19443(8)	0.0314(4)
W12	0.30674(7)	0.32159(5	0.85092(8)	0.0309(4)
P1	0.2682(4)	0.3156(3)	1.0230(4)	0.0164(16)
Cu1	0.5000	0.4397(2)	1.25	0.0350(15)
O1	0.1726(11)	0.2719(8)	1.1435(12)	0.025(5)
O2	0.3015(10)	0.4465(7)	0.9276(10)	0.019(5)
O3	0.1732(10)	0.3745(8)	1.1771(11)	0.025(5)
O4	0.1216(11)	0.4676(8)	1.1188(12)	0.034(6)
O5	0.4380(9)	0.2479(8) 0	0.9916(12) 0	0.026(5)
O6	0.1477(10)	0.3710(9)	0.9348(12)	0.031(6)

(cont. on next page)

Table 4.10. (cont.)

Atom	x	y	z	Ueq
O7	0.4409(11)	0.4507(9)	0.9369(11)	0.032(6)
O8	0.3558(10)	0.4240(8)	1.0450(11)	0.024(5)
O9	0.2929(13)	0.2645(9)	1.1736(10)	0.036(6)
O10	0.5211(10)	0.3074(9)	1.0793(10)	0.025(5)
O11	0.1211(11)	0.3701(8)	1.0545(12)	0.031(5)
O12	0.4267(11)	0.3517(8)	0.9940(13)	0.034(6)
O13	0.1664(10)	0.1817(10)	0.8610(11)	0.032(6)
O14	0.2465(11)	0.3812(7)	0.8479(11)	0.026(5)
O15	0.3581(10)	0.2692(8)	0.8928(14)	0.034(6)
O16	0.0881(9)	0.2682(8)	1.0485(12)	0.027(5)
O17	0.3251(14)	0.3111(11)	0.7757(11)	0.048(8)
O18	0.3737(9)	0.3703(7)	0.8740(9)	0.017(4)
O19	0.2840(10)	0.3508(8)	0.9635(11)	0.028(5)
O20	0.1564(14)	0.1921(10)	0.9958(17)	0.055(8)
O21	0.2776(13)	0.2022(9)	0.9407(13)	0.039(6)
O22	0.3241(10)	0.2795(9)	1.0356(11)	0.029(6)
O23	0.0174(13)	0.3408(8)	0.9679(15)	0.050(8)
O24	0.2581(10)	0.4420(8)	1.1317(12)	0.030(6)
O25	0.2332(10)	0.2764(9)	0.8658(10)	0.028(5)
O26	0.3979(11)	0.3478(8)	1.1165(11)	0.027(5)

(cont. on next page)

Table 4.10. (cont.)

Atom	x	y	z	Ueq
O27	0.1133(11)	0.2735(9)	0.9218(14)	0.041(7)
O28	0.3415(12)	0.1623(9)	1.1760(13)	0.037(6)
O29	0.3915(12)	0.4484(9)	1.1771(14)	0.040(6)
O30	0.2016(12)	0.4352(8)	1.0127(12)	0.034(6)
O31	0.1752(12)	0.4690(9)	0.8806(12)	0.038(6)
O32	0.2578(11)	0.3479(10)	1.0849(15)	0.044(7)
O33	0.2989(11)	0.3650(9)	1.2022(12)	0.033(6)
O34	0.2377(11)	0.1982(9)	1.0973(15)	0.042(7)
O35	0.2072(11)	0.3060(10)	1.2737(12)	0.035(6)
O36	0.4133(11)	0.2451(10)	1.1202(12)	0.037(6)
C16	0.5110(16)	0.5439(12)	1.308(2)	0.034(9)
C17	0.5	0.6847(14)	1.25	0.032(13)
C18	0.514(2)	0.7097(17)	1.181(2)	0.056(12)
C19	0.461(3)	0.1688(13)	1.295(3)	0.067(16)
C20	0.314(3)	0.4354(18)	1.625(3)	0.11(2)
C21	0.514(2)	0.7672(13)	1.1917(15)	0.036(9)
C22	0.463(3)	0.1127(16)	1.2920(18)	0.056(13)

4.2.1.2.4. Results and Discussion for $[Cu(4,4'\text{-bipy})_4][HPW_{12}O_{40}]$

The compound $[Cu(4,4'\text{-bipy})_4][HPW_{12}O_{40}]$ was obtained hydrothermally as purple, plate-like crystals from the reaction of $Na_6[H_2W_{12}O_{40}]$, $CuCl_2.2H_2O$, 4,4'-bipyridine and H_3PO_4.

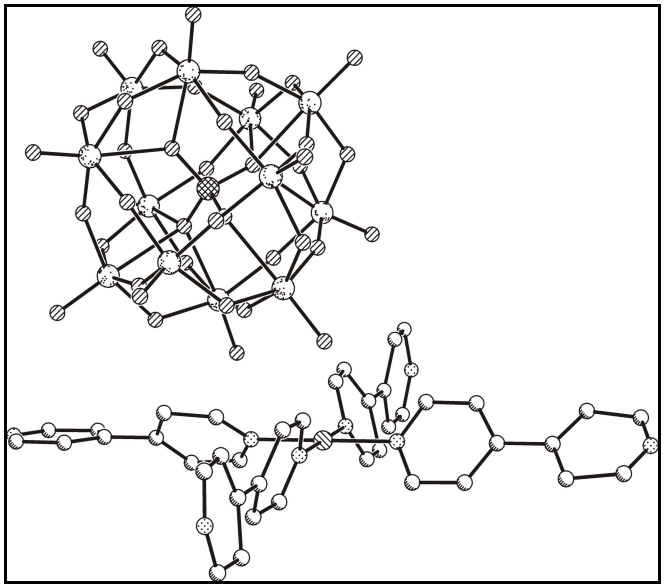

Figure 4.12. View of $[Cu(4,4'\text{-bipy})_4][HPW_{12}O_{40}]$ unit.

The title compound basically consists of Keggin polyanions $[PW_{12}O_{40}]^{3-}$ and $Cu(4,4'\text{-bipy})_4$ complexes as illustrated in Figure 4.12. The $[PW_{12}O_{40}]^{3-}$ polyoxoanion is based on a central PO_4 tetrahedron surrounded by 12 edge- and corner-sharing metal-oxygen octahedra WO_6. The octahedra are arranged in four M_3O_{13} groups. Bond distances found in the WO_6 octahedra can be divided into three groups: W-O_t (terminal bonds) with distances from 1.60(2) to 1.740(19) Å, W-O_b (bridging bonds) ranging from 1.82(2) to 1.98(2) Å and W-O_c (central bonds), varying from 2.41(2) to 2.48(3) Å. Cu is coordinated by four nitrogens from four 4,4'-bipyridine ligands with Cu-N distances from 2.01(3) to 2.06(3) Å. Also Cu has weak interactions with two oxygens of the two discrete Keggin anions and the bond distances of both Cu-O is 2.655 Å. The N-Cu(1)-N bond angles range from 89.9(7) to 179.9(15) °.

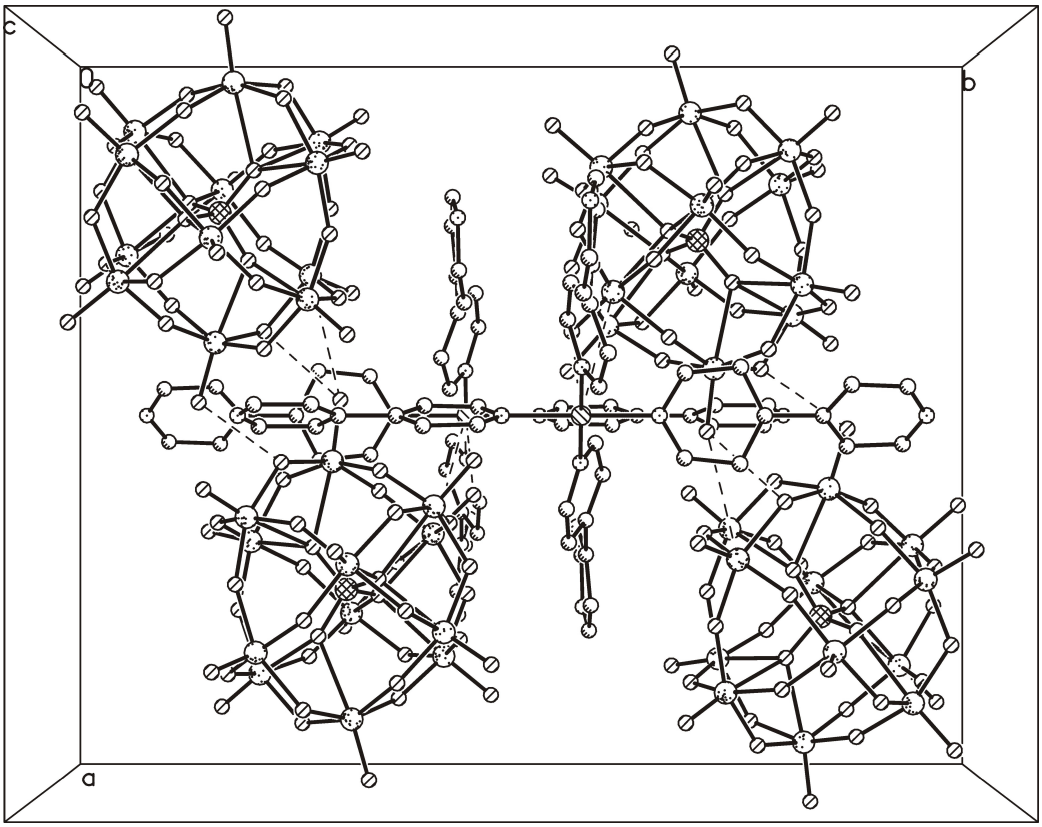

Figure 4.13. Packing view of $[Cu(4,4'\text{-bipy})_4][HPW_{12}O_{40}]$.

The unit cell of the title compound as illustrated in Figure 4.13, consists of four $[PW_{12}O_{40}]^{3-}$ units and two $[Cu(4,4'\text{-bipy})_4]^{2+}$ complexes each having weak interactions with two oxygen atoms of two different polyanions.

The synthesis of these compounds were achieved at pH 2.3. In order to see the effect of pH on POM based compounds, some pH studies were performed. The results of this study showed that even small pH changes had influence on the final products. At different pH values, two of the title compounds, $[Cu(4,4'\text{-bipy})_4][HPW_{12}O_{40}]$ and $(4,4'\text{-bipy})_3[HPW_{12}O_{39}]$, could not be obtained at the same time. The reason for this result can be that POM is very sensitive to $H^{+,}$ so the pH value of the solution can effect the formation process of the final products (Yang et al., 2010).

4.2.1.3. Synthesis and Characterization of $(C_5NH_6)_{4.5}(H_3O)_{1.5}[P_2W_{18}O_{62}]$

Single crystals of $(C_5NH_6)_{4.5}(H_3O)_{1.5}[P_2W_{18}O_{62}]$ were obtained from the reaction of $Na_2WO_4.2H_2O$ (1 mmol, 0.3300 g), $CuCl_2.2H_2O$ (1mmol, 0.1709 g), pyridine (0.37mmol, 0.03 ml), H_3PO_4 (52mmol, 3.5 ml) and H_2O (390mmol, 7 ml). $Na_2WO_4.2H_2O$ (Sigma-Aldrich, 99%), $CuCl_2.2H_2O$ (Merck, 99%), pyridine (Merck, 99%), H_3PO_4 (Sigma-Aldrich, 85%) and H_2O were used without purification.

The reaction mixture was stirred in a teflon vessel for an hour in air and the pH value of the mixture was measured to be almost 0, that indicates a very acidic medium. Then, the solution was transferred to a 23 ml Teflon-lined autoclave and kept at 170 °C for 3 days. After the reaction was finished, the autoclave was cooled to room tempeature slowly. Then, the product was filtered, washed with distilled water and ethanol and dried at room temperature. Transparent, needle-shaped single crystals were obtained (Figure 4.14.).

$$Na_2WO_4.2H_2O + CuCl_2.2H_2O + \text{pyridine} + H_3PO_4 + H_2O$$

$$\xrightarrow[\text{3 days}]{\text{170 °C}}$$

$$(C_5NH_6)_{4.5}(H_3O)_{1.5}[P_2W_{18}O_{62}] \qquad (4.1)$$

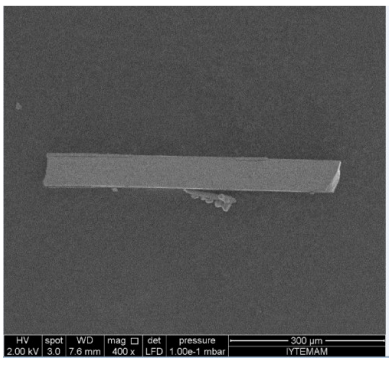

Figure 4.14. SEM image of $(C_5NH_6)_{4.5}(H_3O)_{1.5}[P_2W_{18}O_{62}]$.

The SEM/EDX results of the $(C_5NH_6)_{4.5}$ $(H_3O)_{1.5}[P_2W_{18}O_{62}]$ crystals are shown in Table 4.11. According to the results, the synthesized compound contains tungsten, oxygen carbon, nitrogen and phosphorus elements in the weight percentages of 76.35%, 8.66%, 7.50%, 1.38% and 1.13% respectively.

Table 4.11. SEM/EDX results of $(C_5NH_6)_{4.5}(H_3O)_{1.5}[P_2W_{18}O_{62}]$.

Element	Wt%
C	7.50
N	1.38
O	8.66
P	1.13
W	76.35

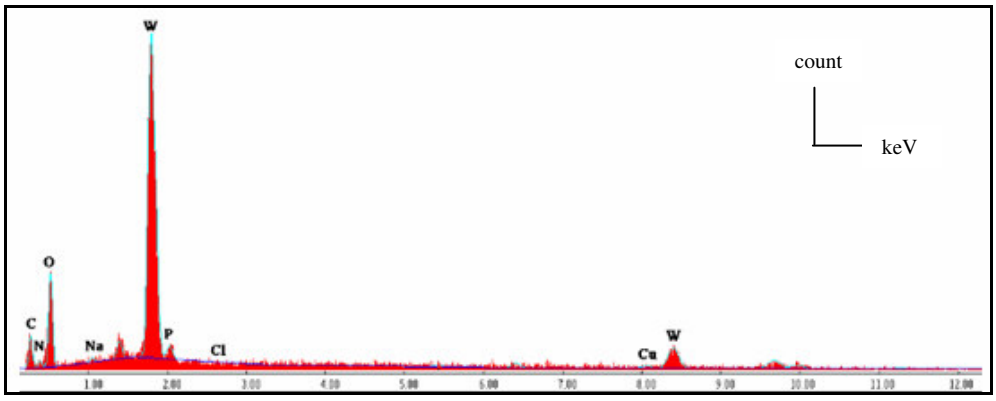

Figure 4.15. SEM/EDX spectrum of $(C_5NH_6)_{4.5}(H_3O)_{1.5}[P_2W_{18}O_{62}]$.

The powder X-ray diffraction pattern of the title compound, which is shown in Figure 4.16, does not match well with any of the compounds in the XRD database. However, after the structure was solved, the compound was found to be a known Dawson polyoxoanion in the literature with the formula $(C_5NH_6)_{4.5}(H_3O)_{1.5}[P_2W_{18}O_{62}]$.

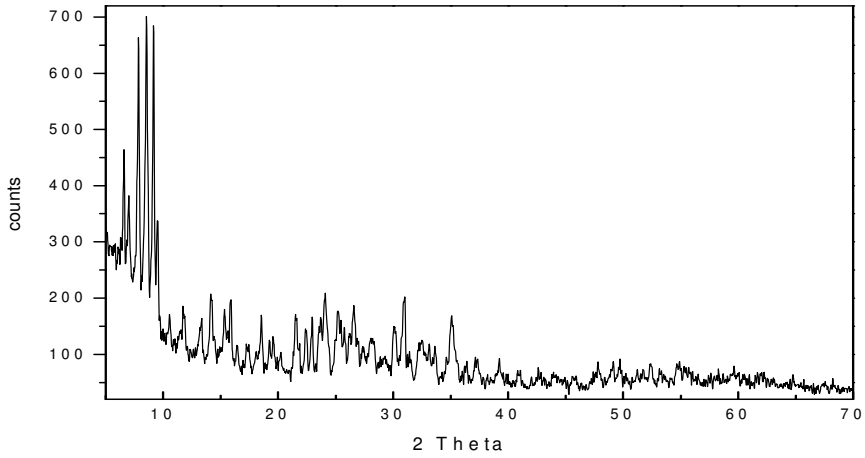

Figure 4.16. Powder pattern of $(C_5NH_6)_{4.5}(H_3O)_{1.5}[P_2W_{18}O_{62}]$.

4.2.1.3.1. X-ray Crystallographic Analysis of $(C_5NH_6)_{4.5}(H_3O)_{1.5}[P_2W_{18}O_{62}]$

Single crystal X-ray diffraction analysis was done for transparent, needle-shaped crystals of $(C_5NH_6)_{4.5}(H_3O)_{1.5}[P_2W_{18}O_{62}]$. The structure of the compound was solved by direct methods using the program SHELXS-97 (Sheldrick, 1990) and by refined full-matrix least-squares techniques using the program SHELXL-97 (Sheldrick, 1997).

Table 4.12. Crystallographic data for $(C_5NH_6)_{4.5}(H_3O)_{1.5}[P_2W_{18}O_{62}]$.

Formula	$(C_5NH_6)_{4.5}(H_3O)_{1.5}[P_2W_{18}O_{62}]$
Formula weight	4752.26
Crystal system	Monoclinic
Space group	C*2/m*
Cell formula units, Z	4
Description	transparent rod-like crystals
Unit cell dimensions	a=26.835(5) Å b=13.960(3) Å c=20.618(4) Å
Volume ($Å^3$)	5397.3(19)

4.2.1.3.2. Results and Discusion for $(C_5NH_6)_{4.5}(H_3O)_{1.5}[P_2W_{18}O_{62}]$

The compound $(C_5NH_6)_{4.5}(H_3O)_{1.5}[P_2W_{18}O_{62}]$ was obtained as transparent, needle-shaped crystals from the hydrothermal reactions of $Na_2WO_4.2H_2O$, $CuCl_2.2H_2O$, pyridine and H_3PO_4.

The title compound includes centrosymmetric $[P_2W_{18}O_{62}]^{6-}$ anion with Dawson structure. $[P_2W_{18}O_{62}]^{6-}$ cluster consists of WO_6 octahedra which are connected to each other with bridging oxygen atoms and two PO_4 tetrahedra inside the cage sharing their oxygen atoms with four of the WO_6 octahedra. The W-O bond distances range from 1.67(2) to 2.37(2) Å according to the characteristics of oxygen atoms being terminal, bridging or central .The P–O distances range from 1.53(2) to 1.65(3) Å.

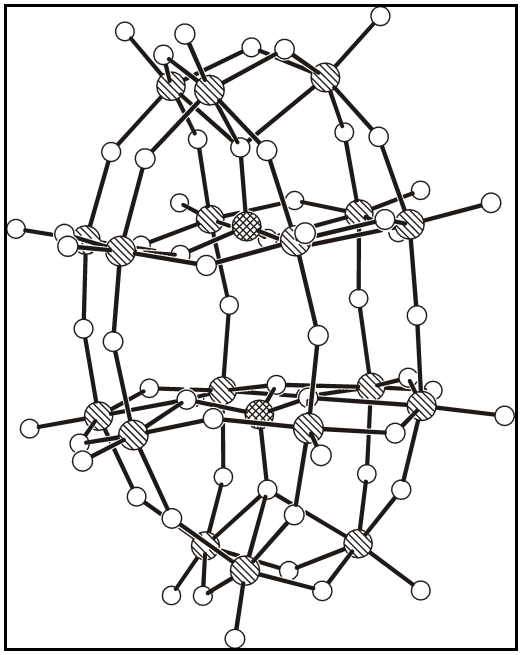

Figure 4.17. View of the $[P_2W_{18}O_{62}]^{6-}$ cage (white: oxygen, black-striped: tungsten, black-crisscrossed: phosphorus).

The whole structure contains hydronium ions and pyridinium cations which interact with the clusters through N-H…..O and O-H….O hyrogen bondings. The hydrogen bondings lead the Dawson units to form into an extended three-dimensional supermolecular network.

The title compound $(C_5NH_6)_{4.5}(H_3O)_{1.5}[P_2W_{18}O_{62}]$ is a known compound which is synthesized before by hydrothermal reactions of pyridine (0.32 ml), $Na_2WO_4.2H_2O$ (0.5 M, 4 ml), H_3PO_4 (0.5 ml, 0.5 M) and H_2O (10 ml) at 313 K in 24 hours and its structure was solved by using the SHELX program (Chen et al., 2008).

CHAPTER 5

CONCLUSION

In the present thesis, hydrothermal synthesis and characterization of transition metal oxide containing organic-inorganic hybrid materials were studied. Vanadium and tungsten transition metals were used in order to construct the inorganic framework of the hybrid structure with phosphate group. The organic components, ethylenediamine, pyridine, 2,2'-bipyridine and 4,4'-bipyridine were used as charge compensating components and/or space filling groups. Hydrothermal reactions of different reactants yielded many crystalline compounds. The obtained compounds were characterized using some microscopic (Optic, SEM) and spectroscopic (FT-IR) techniques. Structures were solved by SHELX program.

One of the synthesized novel compounds is $(H_2NC_4H_8NH_2)[(VO)_2(PO_4)_2]$. The green, plate-like crystals were obtained from the hydrothermal reaction of $NaVO_3$, V_2O_5, ethylenediamine and H_3PO_4 at 170°C for 72 hours in a 23 mL Teflon-lined autoclave. The compound crystallizes in the space group P-*1* of the triclinic system with five formula units in a cell of dimensions a = 6.3345(13) Å, b = 6.3353(13) Å, c = 15.940(3) Å, and V = 639.6(2) $Å^3$. The compound $(H_2NC_4H_8NH_2)[(VO)_2(PO_4)_2]$, exhibits a layered structure with a distance of approximately 7 Å between the layers. The layers are composed of VO_6 octahedra, VO_5 pyramids and PO_4 tetrahedra. Diprotonated piperazine groups exist between these layers.

(4,4'-bipy)$_3$[$HPW_{12}O_{39}$] and [Cu(4,4'-bipy)$_4$][$HPW_{12}O_{40}$] were obtained from the reaction of $Na_6[H_2W_{12}O_{40}]$, $CuCl_2.2H_2O$, 4,4'- bipyridine and H_3PO_4 at pH 2.3, in a 23 ml autoclave at 170°C for 72 hours. The green, rod-like crystals of (4,4'-bipy)$_3$[$HPW_{12}O_{39}$] crystallize in the space group P*2(1)/n* of the monoclinic system with four formula units in a cell with dimensions a = 13.503(3) Å, b = 26.726(5) Å, c = 15.169(3) Å and V = 5397.3(19) $Å^3$. [Cu(4,4'-bipy)$_4$][$HPW_{12}O_{40}$] crystallizes in the space group P*bcn* of the tetragonal system with eight formula units in a cell of dimensions a = 20.236(4) Å, b = 25.635(5) Å, c = 20.236(4) Å; V = 10497(4) $Å^3$. Both compounds are based on Keggin polyoxometalate clusters which contain WO_6 octahedra and a PO_4 tetrahedron at the centre of the cluster. (4,4'-bipy)$_3$[$HPW_{12}O_{39}$]

displays an interesting structure with 1D-chains formed by oxygen sharing $[PW_{12}O_{39}]^{1-}$ clusters and free 4,4'-bipy groups existing among the distinct chains through hydrogen bonding interactions. In $[Cu(4,4'\text{-bipy})_4][HPW_{12}O_{40}]$, $[Cu(4,4'\text{-bipy})_4]^{2+}$ complexes exist between clusters.

A known compound $(VO)(H_2PO_4)_2$ was hydrothermally synthesized as blue, rod-like crystals from the reaction of $NaVO_3$, ethylenediamine and H_3PO_4 at 170°C for 72 hours. The compound crystallizes in the space group P*4/ncc* of the tetragonal system with four formula units in a cell of dimensions a = 8.9633(13) Å, b = 8.9633(13) Å, c = 7.9151(16) Å; V = 635.91(18) $Å^3$. The title compound is composed of layers without organic groups.

The reaction of $Na_2WO_4.2H_2O$, $CuCl_2.2H_2O$, pyridine and H_3PO_4 yielded a known compound $(C_5NH_6)_{4.5}(H_3O)_{1.5}[P_2W_{18}O_{62}]$ as transparent needle-shaped crystals. This compound is a Wells-Dawson polyoxometalate. The compound crystallizes in the space group C*2/m* of the monoclinic system with four formula units in a cell with dimensions a = 26.835(5) Å, b = 13.960(3) Å, c = 20.618(4) Å and the volume is 7531(3) $Å^3$.

As a conclusion, in this study, many experiments were performed, lots of products were obtained and the most significant structures were discussed here. In accordance with the results, it is obvious that hydrothermal method was proven to be an efficient way in order to synthesize novel materials in crystalline form. Thus, the advantages of hydrothermal synthesis combined with introducing different organic ligands yielded vanadium and tungsten oxide containing intriguing organic-inorganic hybrid materials.

REFERENCES

Boudin, S.; Guesdon, A.; Leclaire, A.; Borel, M.-M. Review on Vanadium Phosphates with Mono and Divalent Metallic Cations: Syntheses, Structural Relationships and Classification, Properties. *International Journal of Inorganic Materials.* **2000**, *2*, 561–579.

Byrappa, K.; Yoshimura, M. *Handbook of Hydrothermal Technology: A Technology for Crystal Growth And Materials Processing.* William Andrew: New York, **2001**; pp 1-13.

Chen, Y.; Wang, Y.; Zhang, H.; Yang, Q.; Sun, R.; Cao, Y.; Ni, C. The study of thermal-induced 2D-Cos IR on polyoxomolybdenum (polyoxotungstic). *Journal Of Molecular Structure.* **2008**, *883-884*, 103-108.

Gün, Ö. Hydrothermal synthesis and characterization of ethylenediamine containing molybdenum oxides. M.S.Thesis, İzmir Institute of Technology, İzmir, June 2006.

Hagrman, P. J.; Finn, R. C.; Zubieta, J. Molecular Manipulation of Solid State Structure: Influences of Organic Components on Vanadium Oxide Architectures. *Solid State Sciences.* **2001***, 3*, 745–774.

Jin, H.; Qi, Y.; Wang, E.; Li, Y.; Wang, X.; Qin, C.; Chang, S. Molecular and Multidimensional Organic-Inorganic Hybrids based on Polyoxometalates and Copper Coordination Polymer with Mixed 4,4'-bipyridine and 2,2'-bipyridine Ligands. *Crystal Growth & Design.* **2006**, *6*, 2693-2698.

Borrás-Almenar, J. J.; Coronado, E.; Müller, A. *Polyoxometalate Molecular Science*. Kluwer Academic: Netherlends, 2003.

Kepenekci, Ö. Hydrothermal preparation of single crystalline CeO_2 nanoparticles and the influence of alkali hydroxides on their structure and optical behavior. M.S. Thesis, İzmir Institute of Technology, İzmir, June 2009.

Kozhevnikov, I. V. *Catalysis by Polyoxometalates*. John Wiley & Sons: England, 2002.

Laudise, A. Hydrothermal Synthesis of Crystals. *Chem. Eng. News.* **1987**, *30*, 30-43.

Li, Z.; Lin, B.; Zhang, J.F.; Geng, F.; Han, G.H.; Liu, P.D. Synthesis, Structure and Characterization of An Inorganic–Organic Hybrid Dawson Polyoxotungstate $(H_2en)_3[P_2W_{18}O_{62}]$ $6.48H_2O$. *Journal of Molecular Structure.* **2006**, *783*, 176-183.

Lin, B.Z.; He, L.W.; Xu, B.H.; Li, X.L.; Li, Z.; Liu, P.D. Two Polyoxophosphotungstates Formed by Wells-Dawson Cores Linked through W-O-W Linkages. *Crystal Growth & Design* **2009**, *9*, 273-281.

Martin, W. B.; Martell, A. E. Preparation of Piperazine. *J. Am. Chem Soc.* **1948**, *70*, 1817-1818.

Mutin, P. H.; Guerrero, G.; Vioux, André. Organic–Inorganic Hybrid Materials Based on Organophosphorus Coupling Molecules: From Metal Phosphonates to Surface Modification of Oxides. *C. R. Chimie* .**2003**, *6*, 1153–1164.

Ollivier, P. J.; DeBoard, J. R.D.; Zapf, P.J.; Zubieta, J.; Meyer, L.M.; Wang, C.C.; Mallouk, T.E.; Haushalter, R.C. Hydrothermal Synthesis and Crystal Structures of Two Novel Vanadium Oxides Containing Interlamellar Transition Metal Complexes. *Journal Of Molecular Structure.* **1998***, 470*, 49–60.

Rao, C. N. R., Raveau, B. 1998. Transition metal oxides: Structure, properties and synthesis of ceramic oxides. John Wiley and Sons, New York

Sen, R.; Bera R.; Bhattacharjee A.; Gütlich P.; Ghosh S.; Mukherjee A. K.; Koner S. Oxo-vanadium(IV) Dihydrogen Phosphate: Preparation, Magnetic Study, and Heterogeneous Catalytic Epoxidation. *Langmuir.* **2008**, *24*, 5970-5975.

Smart, L.; Moore, E. A. *Solid State Chemistry: An Introduction.* Taylor & Francis: New York, 2005.

Tanaka J.; Suib S. L. *Experimental Methods In Inorganic Chemistry*. Prentice Hall: New Jersey, 1999.

Schubert, U.; Hüsing, N. *Synthesis of Inorganic Materials* 2nd ed.; Wiley-VCH: Weinheim, 2000.

West A. R. *Solid State Chemistry and Its Applications*. John Wiley & Sons: 1991; England, 1991, pp: 47-100

Yang H.; Lin X.; Xu B.; You Y.; Cao M.; Gao S.; Cao R. Syntheses, structures, and properties of a series of supramolecular hybrids based on Keggin or Wells–Dawson polyoxometalates and 4,4'-bipyridines. *Journal of Molecular Structure.* **2010,** *966*, 33-38.

Zubieta J.; Hagrman P. J.; Hagrman D.. Organic - Inorganic Hybrid Materials: from Simple Coordination Polymers to Organodiamine-Templated Molybdenum Oxides. *Angew. Chem. Int. Ed*. **1999,** *38*, 2638-2684.